Molecular Recognition Directed Self-Assembly of Tubular Liquid Crystalline and Crystalline Supramolecular Architectures from Taper Shaped (15-Crown-5)methyl 3,4,5-Tris(*p*-alkyloxybenzyloxy)benzoates and (15-Crown-5)methyl 3,4,5-Tris(*p*-dodecyloxy)benzoate

Gary Johansson,[a] Virgil Percec*,[a] Goran Ungar[b] and Darija Abramic[b]
[a] *Department of Macromolecular Science, Case Western Reserve University, Cleveland, OH 44106, USA*
[b] *Department of Engineering Materials and Centre for Molecular Materials, The University of Sheffield, Sheffield S1 3DU, UK*

The syntheses and characterization of a series of (15-crown-5)methyl 3,4,5-tris(*p*-alkyloxybenzyloxy)benzoates† with alkyl tails of four **25**, six **26**, and twelve **27** carbon atoms and of (15-crown-5)methyl 3,4,5-tris(*p*-dodecyloxybenzoate) **28** are described. Complexation of the crown ether *endo*-receptor with $NaCF_3SO_3$ destabilizes the crystalline phase of **25**, **26**, **27** and **28** and induces for the case of **27** and **28** the self-assembly of a supramolecular cylindrical channel-like architecture which displays a thermotropic hexagonal columnar (Φ_h) mesophase. Most remarkably, in the crystalline phase of the complexes of **27** with $NaCF_3SO_3$ the cylindrical structure of the Φ_h mesophase is maintained. Characterization of these supramolecular architectures was performed by a combination of differential scanning calorimetry (DSC), thermal optical polarized microscopy, X-ray scattering and molecular modelling. A model is proposed in which a stratum of the column is formed by six molecules of **27** and **28** with the crown ether receptors residing in the column centre and the alkyl tails radiating toward the column periphery. *endo*-Recognition generated *via* the (15-crown-5)methyl receptor upon complexation, and *exo*-recognition provided by the tapered 3,4,5-tris(*p*-dodecyloxybenzyloxy)benzoate and 3,4,5-tris(*p*-dodecyloxy)benzoate fragments of **27** and **28** provide the driving force for the self-assembly of this cylindrical supramolecule.

In a previous paper from our laboratory[1] we have reported that complexation of the crown ether receptor of (benzo-15-crown-5)4′-methyl 3,4,5-tris(*p*-dodecyloxybenzyloxy)benzoate (**DCE**)† with $NaCF_3SO_3$ and KCF_3SO_3 destabilizes its crystalline phase and induces the self-assembly of a supramolecular cylindrical channel-like architecture which displays an enantiotropic thermotropic hexagonal columnar (Φ_h) mesophase. A structural model in which a stratum of the column is formed by an average of 5.8 molecules of **DCE** with the benzo-15-crown-5 receptors placed side by side in the centre of the column and the melted alkyl tails radiating toward its periphery was proposed. *endo*-Recognition generated *via* the benzo-15-crown-5 receptor upon complexation and *exo*-recognition provided by the tapered 3,4,5-tris(*p*-dodecyloxybenzyloxy)benzoate fragment of the self-assembling molecule was suggested as the driving force for the self-assembly of this channel-like supramolecular architecture. The mechanism of self-assembly of this supramolecular architecture was compared to that of tobacco mosaic virus (TMV). The first difference between the self-assembly of TMV from its tapered protein subunits and of our tapered groups consists in the fact that our self-assembled cylindrical structure exists only in the Φ_h mesophase. Upon crystallization, our assembly breaks into a layered structure. TMV maintains its cylindrical shape into its crystalline phase. A crystalline structure which maintains the cylindrical self-assembled supramolecular architecture from the Φ_h mesophase would provide access to a more refined structural characterization of what we suggested to be a channel-like supramolecular architecture.

The goal of this paper is to describe the synthesis and the molecular recognition directed self-assembly of tubular supramolecular architectures from (15-crown-5)methyl 3,4,5-tris(*p*-alkyloxybenzyloxy)benzoates with n-alkyl groups containing four, six, and twelve carbon atoms and from (15-crown-5)-methyl 3,4,5-tris(*p*-dodecyloxy)benzoate. Both series of compounds self-assemble into cylindrical supramolecular architectures *via* principles similar to those described previously.[1,2] The most rewarding result of these experiments is the fact that (15-crown-5)methyl 3,4,5-tris(*p*-dodecyloxybenzyloxy)benzoate maintains its cylindrical shape not only in its Φ_h mesophase but also in its crystalline phase. A mechanism which accounts for this behaviour based on the difference between the conformational flexibility of the benzo-15-crown-5 and (15-crown-5)methyl *endo*-receptors will be presented. This novel system provides a step towards a more refined structural characterization of the supramolecular architectures obtained by the self-assembly of (15-crown-5)methyl 3,4,5-tris(*p*-dodecyloxybenzyloxy)benzoate.

† For convenience, the radical (15-crown-5)methyl is used instead of 2,4,7,10,13-pentaoxacyclopentadecan-2-ylmethyl, the correct term for this entity.

Experimental

Materials.—1-Bromobutane (99%), 1-bromohexane (98%), 1-bromododecane (97%), methyl 4-hydroxybenzoate (99%), lithium aluminium hydride ($LiAlH_4$) (95%), thionyl chloride ($SOCl_2$) (99 + %), tetraethylene glycol (99%), toluene-*p*-sulfonyl chloride (98%), 2,2-dimethyl-1,3-dioxolan-4-ylmethanol (98%), tetrabutylammonium hydrogen sulfate (TBAH) (97%), and potassium *tert*-butoxide (95%) (all from Aldrich) were used as received. Sodium hydride (NaH) (60% dispersion in mineral oil, Aldrich) was washed twice with hexanes immediately before use. Triethylamine (99%, Aldrich) was distilled and stored over solid KOH. Dicyclohexyl-18-crown-6 (DC18C6) (Polysciences) was used as received. Palladium (5% on carbon), and 4-dimethylaminopyridine (DMAP) (97%) (both from Lancaster Synthesis) were used as received. Acetone (A.C.S. reagent grade) and *N*,*N*-dimethylformamide (DMF) (A.C.S. reagent grade) (both from Fisher) were used as received. Tetrahydrofuran

(THF) (A.C.S. reagent grade, Fisher) was refluxed over sodium with benzophenone until the solution turned purple, and then distilled before use. Methylene dichloride (A.C.S. reagent grade, Fisher) was refluxed over CaH_2 and freshly distilled before use. Sodium triflate was prepared as described previously[1] (m.p. 247–249 °C, lit.,[3] m.p. 248 °C).

Techniques.—^{1}H NMR (200 MHz) spectra were recorded on a Varian XL 200 spectrometer with tetramethylsilane (TMS) as internal standard. IR spectra were recorded on a Perkin-Elmer 1320 IR spectrometer. The purity of products was determined by a combination of thin layer chromatography (TLC) on silica gel plates (Kodak) with fluorescent indicator and high pressure liquid chromatography (HPLC) using a Perkin-Elmer Series 10 high-pressure liquid chromatograph equipped with an LC-100 column oven, Nelson Analytical 900 Series integrator data station, and two Perkin-Elmer PL gel columns of 5×10^2 and 1×10^4 Å. THF was used as solvent at the oven temperature of 40 °C. Detection was by UV absorbance at 254 nm. Thermal transitions were measured on a Perkin-Elmer DSC-7 differential scanning calorimeter (DSC). In all cases except where otherwise noted, the heating and cooling rates were 20 °C min^{-1}. The transition temperatures were reported as the maxima and minima of their endothermic and exothermic peaks. Glass transition temperatures (T_g) were read at the midpoint of the change in heat capacity. Indium was used as a calibration standard. X-Ray scattering patterns were recorded using either a helium-filled wide-angle flat plane (WAXS) camera or a pinhole-collimated small-angle (SAXS) camera. Ni-filtered Cu-Kα radiation was used. The temperature stability of the X-ray heating cell was ±0.1 °C. A Carl-Zeiss optical polarized microscope (100× magnification) equipped with a Mettler FP 82 hot stage and a Mettler FP 80 central processor was used to verify thermal transitions and characterize anisotropic textures. Molecular modelling was done using the computer program CSC Chem3D™ from Cambridge Scientific Computing, Inc.

Methyl 4-Butoxybenzoate **5**.—The title compound **5** was synthesized according to a general procedure developed for the synthesis of methyl 4-alkoxybenzoates. Methyl 4-hydroxybenzoate **4** (10.0 g, 0.0657 mol) was dissolved in DMF (100 cm^3) in a round-bottom flask equipped with a magnetic stirrer. The solution was purged for several minutes with nitrogen, after which potassium carbonate (K_2CO_3) (27.2 g, 0.197 mol) and dicyclohexyl-18-crown-6 (DC18C6) (0.24 g, 1.0 mol %) were added to it. To this heterogeneous mixture was added 1-bromobutane **1** (8.55 g, 0.0624 mol) slowly with stirring. The mixture was then heated to 60 °C and stirred for 16 h. The reaction was determined to be complete by TLC (CH_2Cl_2, R_F 0.6) and/or NMR analysis. After cooling to room temperature, the mixture was poured into water (500 cm^3) and the whole then transferred to a separatory funnel and extracted CH_2Cl_2 (2×200 cm^3). The combined organic extracts were washed with dilute HCl (3×100 cm^3) and water (100 cm^3), dried ($MgSO_4$), filtered, and concentrated on a rotary evaporator. The residue was purified by column chromatography (basic alumina, CH_2Cl_2 eluent) to yield a clear oil (10.4 g, 80.1%). Purity (HPLC) 99+%; δ_H($CDCl_3$, TMS) 0.98 (t, 3 H, $CH_3CH_2CH_2CH_2$, J 6.9), 1.48 (m, 2 H, $CH_3CH_2CH_2CH_2$, J 7.5), 1.75 (m, 2 H, $CH_3CH_2CH_2CH_2$, J 7.4), 3.89 (s, 3 H, $PhCO_2CH_3$), 4.01 (t, 6 H, $CH_3CH_2CH_2CH_2$, J 6.9), 6.93 (d, 2 H, *m*-H, J 8.7) and 7.96 (d, 2 H, *o*-H, J 8.9).

Methyl 4-Hexyloxybenzoate **6**.—The title compound **6** was synthesized by the alkylation of **4** (10.0 g, 65.7 mmol) with **2** (10.3 g, 62.4 mmol) according to the general procedure for the synthesis of **5** was obtained as a clear oil (12.7 g, 82.7%); purity (HPLC), 99+%; δ_H($CDCl_3$, TMS) 0.90 [t, 3 H, $CH_3(CH_2)_3CH_2CH_2$, J 5.9], 1.36 [m, 6 H, $CH_3(CH_2)_3CH_2CH_2$], 1.74 [m, 2 H, $CH_3(CH_2)_3CH_2CH_2$], 3.89 (s, 3 H, $PhCO_2CH_3$), 4.01 [t, 2 H, $CH_3(CH_2)_3CH_2$, J 6.8], 6.93 (d, 2 H, *m*-H, J 8.7) and 7.96 (d, 2 H, *o*-H, J 8.6).

Methyl 4-Dodecyloxybenzoate **7**.—The title compound **7** was synthesized by the alkylation of **4** with **3** according to the same procedure as **5** with the following modification. Compound **4** (50.0 g, 0.329 mol) was dissolved in acetone (500 cm^3) in a round-bottom flask equipped with a magnetic stirrer and a reflux condenser. The solution was purged for several minutes with nitrogen after which K_2CO_3 (138 g, 1.00 mol) and DC18C (1.0 g, 0.25 mol %) were added to it. 1-Bromododecane **3** (77.8 g, 0.312 mol) was added slowly with stirring to the heterogeneous mixture which was then heated to reflux. The consumption of **3** was monitored by NMR and the reaction was complete after 16 h. The mixture was cooled to room temperature and filtered and the filtrate was washed with diethyl ether and concentrated on a rotary evaporator. The solid residue was taken up in diethyl ether (300 cm^3) and the solution washed with dilute HCl (2×200 cm^3) and water (200 cm^3), dried ($MgSO_4$), filtered and concentrated on a rotary evaporator. Recrystallization of the residue from hexanes yielded white, sheet-like crystals (73.6 g, 73.6%); purity (HPLC), 99+%; m.p. 56–57 °C (lit.,[4] 54–56.5 °C); δ_H($CDCl_3$, TMS) 0.88 [t, 3 H, $CH_3(CH_2)_9CH_2CH_2$, J 7.3], 1.27 [m, 18 H, $CH_3(CH_2)_9CH_2CH_2$], 1.38 [m, 2 H, $CH_3(CH_2)_9CH_2CH_2$], 3.88 (s, 3 H, $C_6H_4CO_2CH_3$), 4.00 [t, 2 H, $CH_3(CH_2)_9CH_2CH_2$, J 6.8], 6.93 (d, 2 H, *m*-H, J 8.4) and 7.96 (d, 2 H, *o*-H, J 8.7).

4-Butoxybenzyl Alcohol **8**.—The title compound **8** was synthesized according to a general procedure developed for the $LiAlH_4$ reduction of methyl 4-alkoxybenzoates. $LiAlH_4$ (1.82 g, 0.0480 mol) was suspended in dry THF (100 cm^3) and the solution cooled to 0 °C in a round-bottom flask equipped with a mechanical stirrer and addition funnel. Compound **5** (10.0 g, 0.0480 mol) in THF (50 cm^3) was added dropwise to the stirred suspension. After complete addition, the viscous mixture was allowed to warm to room temperature and then stirred for 2 h. The reaction was quenched by the slow addition of water from the addition funnel to the mixture until hydrogen evolution ceased. The reaction mixture was concentrated on a rotary evaporator and the resultant solid stirred in water (500 cm^3). The suspension was acidified with dilute HCl and extracted with diethyl ether (2×300 cm^3). The combined extracts were washed with water (200 cm^3), dried ($MgSO_4$), filtered, and concentrated on a rotary evaporator. The resultant oil which solidified on cooling was purified by vacuum distillation to yield **8** as a clear oil (7.37 g, 85.3%) which solidified on cooling; purity (HPLC), 99+%; m.p. 31–33 °C (lit.,[5] 32–32.5 °C); δ_H($CDCl_3$, TMS) 0.98 (t, 3 H, $CH_3CH_2CH_2CH_2$, J 7.4), 1.51 (m, 2 H, $CH_3CH_2CH_2CH_2$, J 7.0), 1.77 (m, 2 H, $CH_3CH_2CH_2CH_2$, J 7.4) 3.47 (br s, 1 H, CH_2OH), 3.96 (t, 2 H, $CH_3CH_2CH_2CH_2$, J 7.0), 4.59 (d, 2 H, $PhCH_2OH$, J 4.7), 6.91 (d, 2 H, *m*-H J 8.3) and 7.27 (d, 2 H, *o-H*, J 7.9).

4-Hexyloxybenzyl Alcohol **9**.—The title compound **9** was synthesized by the reduction of **6** (12.7 g, 53.8 mmol) with $LiAlH_4$ according to the general procedure described for the synthesis of **8**. After extraction and removal of solvent a low melting point solid was obtained (10.7 g, 95.6%), the further purification of which was unnecessary; purity (HPLC), 99+%; m.p. 34–36 °C; δ_H($CDCl_3$, TMS) 0.90 [t, 3 H, $CH_3(CH_2)_3CH_2CH_2$, J 5.7], 1.36 [m, 6 H, $CH_3(CH_2)_3CH_2CH_2$], 1.74 [m, 2 H, $CH_3(CH_2)_3CH_2CH_2$], 3.95 [t, 2 H, $CH_3(CH_2)_3CH_2CH_2$, J 6.8], 4.61 (d, 2 H, $PhCH_2OH$, J 5.0), 6.90 (d, 2 H, *m*-H, J 8.6) and 7.25 (d, 2 H, *o*-H, J 8.4).

4-*Dodecyloxybenzyl Alcohol* **10**.—The title compound **10** was synthesized by the reduction of **7** (50.0 g, 0.156 mol) with $LiAlH_4$ according to the general procedure described for the synthesis of **8**. After extraction and removal of solvent a white solid was obtained (43.0 g, 96.3%); purity (HPLC), 99+%; m.p. 66–68 °C (lit.,[6] 59–60 °C); δ_H($CDCl_3$, TMS) 0.88 [t, 3 H, $CH_3(CH_2)_9CH_2CH_2$, *J* 4.9], 1.26 [m, 18 H, $CH_3(CH_2)_9CH_2$-CH_2], 1.77 [m, 2 H, $CH_3(CH_2)_9CH_2CH_2$], 3.95 [t, 2 H, $CH_3(CH_2)_9CH_2CH_2$, *J* 6.6], 4.60 (s, 2 H, $PhCH_2OH$), 6.90 (d, 2 H, *m*-H, *J* 8.6) and 7.25 (d, 2 H, *o*-H, *J* 8.5).

4-*Butoxybenzyl Chloride* **11**.—The title compound **11** was synthesized according to a general procedure developed for the preparation of 4-alk benzyl chlorides from the corresponding 4-alkoxybenzyl alcohols. Compound **8** (25.0 g, 0.139 mol) was dissolved in dry CH_2Cl_2 (125 cm^3) in a round-bottom flask equipped with a stirrer and $SOCl_2$ (19.9 g, 0.167 mol) was added slowly to the solution over several minutes. Immediately after addition, an aliquot was removed for analysis. The NMR spectrum [δ 4.58 (d, 2 H, $PhCH_2OH$) disappeared, δ 4.55 (s, 2 H, $PhCH_2Cl$) appeared] and the TLC ($CHCl_3$, R_F 0.9) analysis indicated complete conversion. The solvent was removed on a rotary evaporator at room temperature and residual $SOCl_2$ was removed under high vacuum for several hours at room temperature to yield **11** as a light yellow oil (27.0 g, 97.7%). It was used immediately with no further purification.

4-*Hexyloxybenzyl Chloride* **12**.—The title compound **12** was synthesized according to the general procedure described for **11** starting from **9** (6.40 g, 29.8 mmol); yield 6.40 g (100%).

4-*Dodecyloxybenzyl Chloride* **13**.—The title compound **13** was synthesized according to the same general procedure described for **11** starting from **10** (43.0 g, 0.156 mol); yield 46.0 g (94.9%).

3,4,5-*Tris*(p-*butoxybenzyloxy*)*benzoic Acid* **15**.—The title compound **15** was synthesized according to a modification of a general procedure developed for the alkylation of methyl 3,4,5-trihydroxybenzoate **14** and the subsequent hydrolysis of the methyl ester.[7] Compound **14** (5.0 g, 0.0272 mol) was dissolved in DMF (150 cm^3) in a round-bottom flask equipped with a stirrer and a $CaCl_2$ drying tube. The solution was purged for several minutes with nitrogen after which K_2CO_3 (33.9 g, 0.245 mol) was added to it and the heterogeneous mixture stirred vigorously. Compound **11** (15.7 g, 0.163 mol) was added slowly to the mixture and the reaction temperature was raised to 60 °C. The DMF solution turned dark brown during the reaction. After 8 h, the consumption of **11** was shown to be complete by TLC (THF, R_F 0.7) analysis. The mixture was cooled to room temperature and poured into water. The precipitated solid was filtered off and dissolved in CH_2Cl_2 (200 cm^3) and the solution was washed with dilute HCl (3 × 150 cm^3) and water (×2), dried ($MgSO_4$), filtered and concentrated on a rotary evaporator. The resultant crude product was purified by flash column chromatography (basic alumina, THF) and recrystallized from propan-1-ol to yield a white solid (13.7 g, 75.0%). KOH (8.4 g, 0.15 mol) was dissolved in 95% EtOH/water (3:1; 150 cm^3) in a round-bottom flask equipped with a mechanical stirrer and a reflux condenser. The methyl ester of **15** (13.0 g, 0.0193 mol) was added to the mixture which was then heated to reflux. The potassium salt was precipitated from the solution during the course of the hydrolysis. After 3 h, the hydrolysis was complete (TLC; CH_2Cl_2, R_F < 0.1). The reaction mixture was cooled to room temperature and the ethanol removed on a rotary evaporator. The aqueous suspension was poured into water (500 cm^3) and the mixture cooled to 0 °C and acidified with 1 mol dm^{-3} HCl. The aqueous mixture was extracted with CH_2Cl_2 containing TBAH (0.05 g). The organic extracts were washed with water (200 cm^3), dried ($MgSO_4$), filtered, and the solvent removed on a rotary evaporator. Recrystallization of the residue from propanol yielded the title compound **15** as a white powder (10.6 g, 83.6%). Thermal transitions (°C) and enthalpy changes of transitions (kcal mol^{-1}) are (DSC): k 131 (1.30) k 147 (12.5) i on heating; i 101 (overlapped transition) Φ_h 98 (4.53) k on cooling; δ_H($CDCl_3$, TMS) 0.98 (t, 9 H, $CH_3CH_2CH_2CH_2$, *J* 7.5), 1.52 (m, 6 H, $CH_3CH_2CH_2CH_2$), 1.78 (m, 6 H, $CH_3CH_2CH_2CH_2$), 3.95 (t, 2 H, $CH_3CH_2CH_2$-CH_2 from 4-position, *J* 7.5), 3.95 (t, 4 H, $CH_3CH_2CH_2CH_2$ from 3- and 5-position, *J* 6.7), 5.04 (s, 2 H, $PhCH_2O$ from 4-position), 5.06 (s, 4 H, $PhCH_2O$ from 3- and 5-position), 6.79 (d, 2 H, *m*'-H, *J* 8.7), 6.93 (d, 4 H, *m*-H, *J* 9.0), 7.24 (d, 2 H, *o*'-H, *J* 8.4), 7.32 (d, 4 H, *o*-H, *J* 8.5), 7.43 (s, 2 H, 2- and 6-ArH).

3,4,5-*Tris*(p-*hexyloxybenzyloxy*)*benzoic Acid* **16**.—The title compound **16** was synthesized from **14** (1.83 g, 9.93 mmol) and **12** (6.40 g, 29.8 mmol) according to the general procedure described for the synthesis of **15**. The reaction mixture when poured into MeOH gave a white powder (4.18 g, 58.3%). Hydrolysis of the methyl ester followed by recrystallization from propan-1-ol yielded a white powder (3.47 g, 84.7%). Thermal transitions (°C) and enthalpy changes of transitions (kcal mol^{-1}) are (DSC): k 132 (11.5) k 140 (2.63) i on heating, i 118 (1.29) Φ_h 53 (1.84) k; δ_H($CDCl_3$, TMS) 0.91 [t, 9 H, $CH_3(CH_2)_3CH_2CH_2$, *J* 5.6], 1.37 [m, 18 H, $CH_3(CH_2)_3$-CH_2CH_2], 1.76 (m, 6 H, $CH_3(CH_2)_3CH_2CH_2$], 3.93 [t, 2 H, $CH_3(CH_2)_3CH_2CH_2$ from 4-position, *J* 6.6], 3.97 (t, 4 H, $CH_3(CH_2)_3CH_2CH_2$ from 3- and 5-positions, *J* 6.5), 5.04 (s, 2 H, $PhCH_2O$ from 4-positions), 5.06 (s, 4 H, $PhCH_2O$ from 3- and 5-positions), 6.79 (d, 2 H, *m*'-H, *J* 9.1), 6.93 (d, 4 H, *m*-H, *J* 8.5), 7.27 (d, 2 H, *o*'-H, *J* 8.4), 7.32 (d, 4 H, *o*-H, *J* 8.6) and 7.42 (s, 2 H, 2- and 6-H).

3,4,5-*Tris*(p-*dodecyloxybenzyloxy*)*benzoic Acid* **17**.—The synthesis and purification of **17** has been reported previously.[7] In this case the procedure was modified according to the general procedure described for the synthesis of **15** starting from **14** (9.2 g, 0.050 mol) and **13** (46.0 g, 0.148 mol). Recrystallization from propan-1-ol yielded a white powder (28.5 g, 70.3%). Thermal transitions (°C) and enthalpy changes of transitions (kcal mol^{-1}) are (DSC): k 73 (13.5) Φ_h 136 (1.57) i on heating (lit.,[7a] k 66 Φ_h 137 i), i 126 (1.78) Φ_h 33 (overlapped transition) k 24 (7.00) k on cooling.

3,4,5-*Tri*(*dodecyloxy*)*benzoic Acid* **18**.—The synthesis and purification of **18** has been described previously.[7]

3,6,9-*Trioxaundecane*-1,11-*diyl Ditoluene*-p-*sulfonate* **20**.—Compound **20** was synthesized according to a literature procedure.[8] 3,6,9-Trioxaundecane-1,11-diol (tetraethylene glycol) **19** (25.0 g, 0.129 mmol) and triethylamine (35.5 g, 0.351 mol) were dissolved in dry CH_2Cl_2 (50 cm^3) in a round bottom flask equipped with a magnetic stirrer, nitrogen inlet–outlet, thermometer, and dropping funnel. The solution was cooled to 0 °C on an ice–water bath and toluene-*p*-sulfonyl chloride (54.0 g, 0.283 mol) in CH_2Cl_2 (200 cm^3) was added over 2 h to the solution, the temperature being maintained < 10 °C. The solution was warmed to room temperature, stirred for 26 h, and diluted with CH_2Cl_2 (300 cm^3). The reaction mixture was washed with water (300 cm^3), 10% HCl (200 cm^3), and saturated aqueous $NaHCO_3$ (200 cm^3). The organic extracts were dried ($MgSO_4$), filtered, and the solvent removed on a rotary evaporator. The yellow oil was purified by column chromatography (silica gel, diethyl ether) to yield a clear oil (52.2 g, 80.6%). Purity (HPLC), 99+%; δ_H($CDCl_3$, TMS) 2.44 (s, 6 H, $CH_3C_6H_4$), 3.56 (s, 8 H, $CH_2CH_2OCH_2CH_2$), 3.68 (t, 4 H, *p*-

$TsOCH_2CH_2$, *J* 4.9), 4.16 (t, 4 H, *p*-$TsOCH_2CH_2CH_2$, *J* 5.0), 7.37 (d, 4 H, 3- and 5-ArH, *J* 8.5) and 7.78 (d, 4 H, 2- and 6-ArH, *J* 7.9).

(±)-3-*Benzyloxypropane*-1,2-*diol* **22**.—Compound **21** (25.0 g, 0.189 mol) and potassium *tert*-butoxide (24.5 g, 0.218 mol) were dissolved in dry THF (145 cm^3) in a round bottom flask equipped with a mechanical stirrer, condenser, addition funnel, and nitrogen inlet–outlet. The heterogeneous reaction mixture turned green and after it had been heated to reflux, benzyl bromide (32.4 g, 0.189 mol) in THF (45 cm^3) was added dropwise to it. During the addition, a precipitate formed and the mixture turned yellow. After 28 h, GLC analysis indicated only 80% conversion of the mixture and, subsequently, an excess of potassium *tert*-butoxide (5.0 g, 0.045 mol) was added to it; after 1 h, GLC analysis indicated complete conversion. The mixture was cooled to room temperature and filtered. The solids were washed with CH_2Cl_2 and the solvent was removed on a rotary evaporator to yield a yellow oil (39.0 g, 92.8%). Purity (GLC), 92.0% (4% benzyl bromide, 4% **21**). The oil was dissolved in THF (80 cm^3) and 1 mol dm^{-3} HCl (80 cm^3) and the solution was stirred at room temperature for 12 h; after this time no acetal was detected by GLC. The product was extracted into CH_2Cl_2 (200 cm^3), washed twice with water, dried ($MgSO_4$), filtered, and the solvent removed on a rotary evaporator to give a yellow oil. The product was fractionally distilled twice *in vacuo*, b.p. 123–127 °C at 0.25 mmHg (lit.,[9] 141–143 °C at 0.8 mmHg) to yield a clear oil (11.9 g, 34.6%). Purity (GLC), 99+%; δ_H($CDCl_3$, TMS) 2.77 (br s, 2 H, OH), 3.55 [overlapped d, 4 H, $OCH_2CH(OH)CH_2OH$], 3.89 [m, 1 H, CH(OH)], 4.54 (s, 2 H, $PhCH_2$) and 7.34 (s, 5 H, benzyl).

Benzyl 2,4,7,10,13-*Pentaoxacyclopentadecan*-2-*ylmethyl Ether* **23**.—The synthesis and purification of compound **23** was performed as described previously starting from **20** (32.8 g, 65.3 mmol) and **22** (11.9 g, 65.3 mmol).[10] After purification by column chromatography (neutral alumina, 10% propan-2-ol–hexanes) **23** as a pink oil was isolated (5.06 g, 22.8%). Purity (HPLC), 97%; δ_H($CDCl_3$, TMS) 3.55 [overlapped d, 4 H, $PhCH_2OCH_2CH(OCH_2CH_2)CH_2O$, *J* 4.6], 3.67 (overlapped peaks, 17 H, OCH_2CH_2, $PhCH_2OCH_2CH$), 4.55 (s, 2 H, $PhCH_2O$) and 7.33 (m, 5 H, $PhCH_2$).

2,4,7,10,13-*Pentaoxacyclopentadecan*-2-*ylmethanol* **24**.—Compound **23** (5.06 g, 15.5 mmol) was dissolved in 95% EtOH (75 cm^3) in a pressure flask. 5% Palladium-on-carbon (10 wt%; 0.5 g) was added to the solution and the benzyl ether was hydrogenolysed on a Parr hydrogenator, equipped with a shaker, at 60 psi for 16 h at room temperature. The reaction mixture was filtered through diatomaceous earth and the solvent was removed on a rotary evaporator to yield a pink oil (3.86 g, 100%); δ_H($CDCl_3$, TMS) 3.67 (m, 22 H).

2,4,7,10,13-*Pentaoxacyclopentadecan*-2-*ylmethyl* 3,4,5-*Tris*-(p-*butoxybenzyloxy*)*benzoate* **25**.—The following method was developed in our laboratory.[2c] Compounds **24** (0.76 g, 3.1 mmol) and **15** (2.0 g, 3.1 mmol) were dissolved in THF (40 cm^3) in a round bottom flask equipped with a magnetic stirrer. K_2CO_3 (2.1 g, 15 mmol), DMAP (0.076 g, 20 mol %), toluene-*p*-sulfonyl chloride (0.58 g, 3.1 mmol), and TBAH (0.21 g, 20 mol %) were added to the mixture which was then stirred for 16 h at room temperature. The reaction mixture was filtered and the solvent was removed on a rotary evaporator. The crude product was dissolved in CH_2Cl_2 (50 cm^3) and the solution washed with dilute HCl (50 cm^3) and water (50 cm^3), dried ($MgSO_4$), filtered, and concentrated on a rotary evaporator. Purification by flash column chromatography (basic alumina, THF) and precipitation from CH_2Cl_2 into MeOH yielded a white solid (1.26 g, 46.6%). Purity (HPLC), 99%; m.p. 67 °C (DSC, 20 °C min^{-1}); δ_H($CDCl_3$, TMS) 0.98 (t, 9 H, $CH_3CH_2CH_2CH_2$, *J* 7.5), 1.48 (q, 6 H, $CH_3CH_2CH_2CH_2$, *J* 7.7), 1.78 (m, 6 H, $CH_3CH_2CH_2CH_2$), 3.68 (m, 16 H, OCH_2CH_2O), 3.78 [overlapped peak, 2 H, $OCH_2CH(OR)CH_2O$], 3.84 [overlapped peak, 1 H, $OCH(CH_2OR)CH_2O$], 3.94 (overlapped t, 6 H, $CH_3CH_2CH_2CH_2$ from internal and external phenyl), 4.30 [dd, 1 H, $CO_2CH_a(H_b)CH_c(OR)CH_2O$, J_{ab} 11.8, J_{ac} 5.6], 4.39 [dd, $CO_2CH_b(H_a)CH_c(OR)CH_2O$, J_{ab} 11.8, J_{bc} 4.9], 5.01 (s, 2 H, $PhCH_2O$ on internal benzyl), 5.04 (s, 4 H, $PhCH_2O$ on external benzyl), 6.78 (d, 2 H, *m*′-H, *J* 8.8), 6.92 (d, 4 H, *m*-H, *J* 8.6), 7.28 (d, 2 H, *o*′-H, *J* 8.6), 7.35 (d, 4 H, *o*-H, *J* 8.8), 7.36 (s, 2 H, 2- and 6-H).

2,4,7,10,13-*Pentaoxocyclopentadecan*-2-*ylmethyl* 3,4,5-*Tris*-(p-*hexyloxybenzyloxy*)*benzoate* **26**.—Compound **26** was synthesized by the esterification of compound **16** (1.23 g, 1.66 mmol) with compound **24** (0.415 g, 1.66 mmol) according to the general procedure described for the synthesis of **25**. Two recrystallizations from MeOH–propan-2-ol (2:1), gave a white powder (0.68 g, 43.8%). Purity (HPLC), 98%; m.p. 78 °C (DSC, 20 °C min^{-1}); δ_H($CDCl_3$, TMS) 0.91 [t, 9 H, $CH_3(CH_2)_3CH_2CH_2$, *J* 5.1], 1.36 [m, 18 H, $CH_2(CH_2)_3CH_2CH_2$], 1.78 [m, 6 H, $CH_3(CH_2)_3CH_2CH_2$], 3.68 (m, 16 H, OCH_2CH_2O), 3.78 [overlapped peak, 2 H, $OCH_2CH(OR)CH_2O$], 3.84 [overlapped peak, 1 H, $OCH(CH_2OR)CH_2O$], 3.96 [overlapped t, 6 H, $CH_3(CH_2)_3CH_2CH_2$ from internal and external benzyl], 4.30 [dd, 1 H, $CO_2CH_a(H_b)CH_c(OR)CH_2O$, J_{ab} 11.8, J_{ac} 5.6], 4.39 [dd, $CO_2CH_b(H_a)CH_c(OR)CH_2O$, J_{ab} 11.8, J_{bc} 4.9], 5.01 (s, 2 H, $PhCH_2O$ on internal benzyl), 5.04 (s, 4 H, $PhCH_2O$ on external benzyl), 6.79 (d, 2 H, *m*′-H, *J* 8.8), 6.92 (d, 4 H, *m*-H *J* 8.0), 7.28 (d, 2 H, *o*′-H, *J* 8.1), 7.35 (d, 4 H, *o*-H, *J* 8.2) and 7.36 (s, 2 H, 2-and 6-H).

2,4,7,10,13-*Pentaoxacyclopentadecan*-2-*ylmethyl* 3,4,5-*Tris*-(p-*dodecyloxybenzyloxy*)*benzoate* **27**.—Compound **27** was synthesized by the esterification of compound **17** (3.18 g, 3.27 mmol) with compound **24** (0.80 g, 3.20 mmol) according to the general procedure described for the synthesis of **25**. Recrystallization from propan-1-ol–MeOH (3:2), gave a white powder (2.04 g, 51.8%). Purity (HPLC), 99%; m.p. 60 °C (DSC, 20 °C min^{-1}); δ_H($CDCl_3$, TMS) 0.88 [t, 9 H, $CH_3(CH_2)_9CH_2CH_2$, *J* 6.5], 1.27 [m, 54 H, $CH_3(CH_2)_9CH_2CH_2$], 1.79 (m, 6 H, $CH_3(CH_2)_9CH_2CH_2$], 3.68 (m, 16 H, OCH_2CH_2O), 3.78 [overlapped peak, 2 H, $OCH_2CH(OR)CH_2O$], 3.84 [overlapped peak, 1 H, $OCH(CH_2OR)CH_2O$], 3.96 [overlapped t, 6 H, $CH_3(CH_2)_9CH_2CH_2$ from internal and external benzyl], 4.30 [dd, 1 H, $CO_2CH_a(H_b)CH_c(OR)CH_2O$, J_{ab} 11.6, J_{ac} 5.8], 4.39 [dd, $CO_2CH_b(H_a)CH_c(OR)CH_2O$, J_{ab} 11.8, J_{bc} 5.3], 5.01 (s, 2 H, $PhCH_2O$ on internal benzyl), 5.04 (s, 4 H, $PhCH_2O$ on external benzyl), 6.78 (d, 2 H, *m*′-H, *J* 9.3), 6.91 (d, 4 H, *m*-H, *J* 8.8), 7.28 (d, 2 H, *o*′-H, *J* 8.0) and 7.36 (overlapped peaks, 6 H, *o*-H, *J* 8.2, 2- and 6-H).

2,4,7,10,13-*Pentaoxacyclopentadecan*-2-*ylmethyl* 3,4,5-*Tris*-(*dodecyloxy*)*benzoate* **28**.—Compound **28** was synthesized by the esterification of compound **18** (1.8 g, 2.7 mmol) with compound **24** (0.68 g, 2.7 mmol) according to the general procedure described for the synthesis of compound **25**. Recrystallization from MeOH–CH_2Cl_2 (10:1) gave a low melting point solid (1.21 g, 49.4%). Purity (HPLC), 98%; m.p. (DSC, 20 °C min^{-1}), 32 °C; δ_H($CDCl_3$, TMS) 0.88 [t, 9 H, $CH_3(CH_2)_9CH_2CH_2$, *J* 6.3], 1.27 [m, 54 H, $CH_3(CH_2)_9CH_2CH_2$], 1.78 [m, 6 H, $CH_3(CH_2)_9CH_2CH_2$], 3.68 (m, 19 H, crown ether H), 4.01 [t, 6 H, $CH_3(CH_2)_9CH_2CH_2$, *J* 6.3], 4.34 [dd, 1 H, $OCH_a(H_b)CH_c(OR)CH_2O$, J_{ab} 12.1, J_{ac} 6.5], 4.41 [dd, 1 H, $OCH_a(H_b)CH_c(OR)CH_2O$, J_{ab} 11.5, J_{bc} 4.9] and 7.26 (s, 2 H, 2- and 6-H).

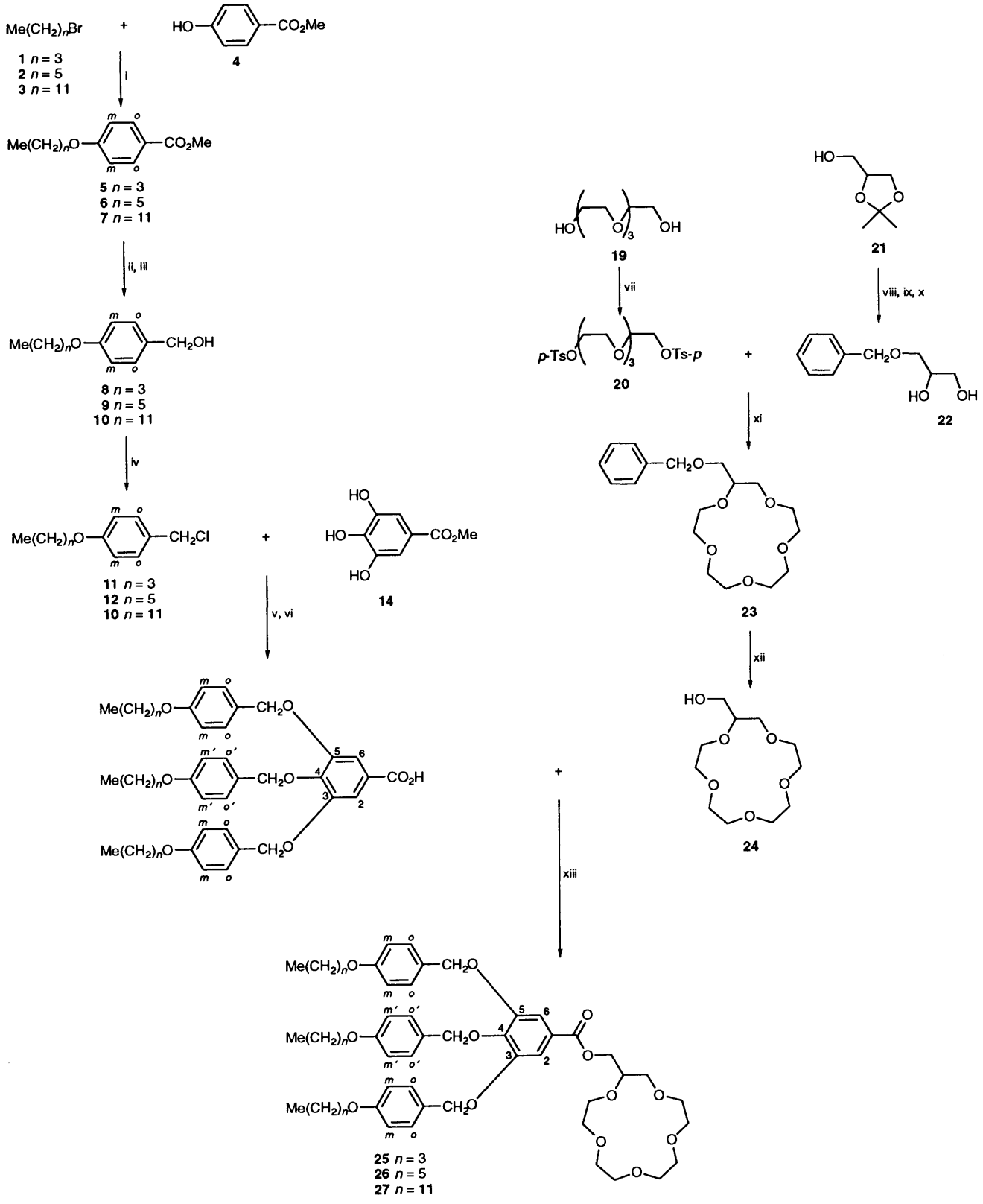

Scheme 1 Synthesis of compounds **25**, **26** and **27**. *Reagents and conditions:* i, K_2CO_3, DC18C_6, acetone, reflux; ii, $LiAlH_4$, THF, 0 °C; iii, H_2O; iv, $SOCl_2$, $CHCl_2$, room temp.; v, K_2CO_3, DMF, 60 °C; vi, 1 mol dm^{-1} KOH/95% EtOH; vii, *p*-TsCl, Et_3N, CH_2Cl_2, 0 °C; viii, KOBu^t, THF, reflux; ix, $PhCH_2Br$; x, 5% HCl, THF, 25 °C; xi, NaH, THF, reflux; xii, H_2, Pd/C, 60 psi, 95% EtOH, room temp.; xiii, K_2CO_3, *p*-TsCl, DMAP, TBAH, THF, room temp.

Results and Discussion

Scheme 1 outlines the synthesis of compounds **25**, **26** and **27**. The synthesis of compound **17** has been described previously in the literature starting from *p*-hydroxybenzaldehyde.[7] However, in these experiments, methyl 4-hydroxybenzoate was used as a starting material for the synthesis of compounds **15**, **16** and **17** because of its availability in high purity and its resistance to oxidation during storage and manipulation.

In a previous study, 4′-hydroxymethylbenzo(15-crown-5) was chosen as the precursor for the esterification of the

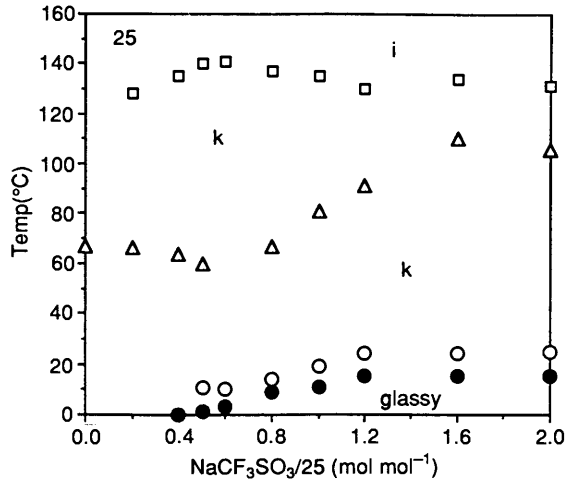

Fig. 1 The dependence of the phase transition temperatures of the complexes of **25** with $NaCF_3SO_3$ on the $NaCF_3SO_3$/**25** molar ratio. Data from the first heating scan: ΔT_{k1-k2}; □ T_{k2-i}. Data from the first cooling scan: ● T_g. Data from the second heating scan: ○ T_g.

benzo(15-crown-5) *endo*-receptor to the tapered *exo*-receptor **17** because it maintains an electron-donating substituent on the macrocycle. This functional group does not decrease the complexation ability of the 15-crown-5 receptor.[11] Even more recently, self-assembled systems derived from the esterification products of oligooxyethylenic *endo*-receptors with the tapered *exo*-receptors were described.[2c] In this study, (±)-hydroxymethyl(15-crown-5) **24** was chosen as the *endo*-receptor.

Compound **24** is the macrocyclic analogue of pentaethylene glycol and is more flexible than the benzo(15-crown-5) moiety. No thermodynamic data for complexes of **24** and 4′-hydroxymethylbenzo(15-crown-5) with sodium cations under comparable conditions are available. However, equilibrium constants (log K_e) for complexation of **24**[10] and benzo(15-crown-5)[12] with sodium cations in 90% aqueous MeOH solution, where conformational effects should be minimized, are identical. Therefore, any differences in the phase behaviour of the resultant complexes derived from **24** and benzo(15-crown-5) should result from differences in the conformational flexibility of the two macrocycles and not from differences in their electronic nature. Compound **24** was synthesized in good overall yield starting from (±)-2,2-dimethyl-1,3-dioxolan-4-ylmethanol **21** and tetraethylene glycol ditosylate. Protection of **21** with benzyl bromide followed by acid-catalysed hydrolysis of the resultant dimethyl acetal at room temperature afforded (±)-3-benzyloxypropane-1,2-diol **22** in excellent yield. The cyclization was carried out using a modified Pedersen[13] crown ether synthesis to afford (±)-benzyloxymethyl(15-crown-5) **23** in fair yield. Subsequent hydrogenolysis yielded **24**. Esterification of **24** with a series of 3,4,5-tris(*p*-alkyloxybenzyloxy)benzoic acids under mildly basic conditions afforded the desired macroreceptors in good yield. An alternative method of esterification using dicyclohexylcarbodiimide (DCC) in the presence of *N*,*N*-dimethylaminopyridinium toluene-*p*-sulfonate (DPTS) leads to somewhat higher yields and has been described previously.[1]

Scheme 2 outlines the synthesis of (15-crown-5)methyl 3,4,5-tris(*p*-dodecyloxy)benzoate **28**. Previous experiments in our laboratory,[1,2c] have shown that the benzyl ether moieties of 3,4,5-tris(*p*-dodecyloxybenzyloxy)benzoates undergo thermal decomposition at high temperatures. Therefore, it is desirable to study the phase behaviour of a thermally stable macroreceptor derived from 3,4,5-tris(*p*-dodecyloxy)benzoic acid **18**.

The phase behaviour of compounds **25**–**28** and of their complexes with sodium triflate ($NaCF_3SO_3$) has been studied by a combination of DSC, thermal polarized optical microscopy and small and wide-angle X-ray scattering experiments. The

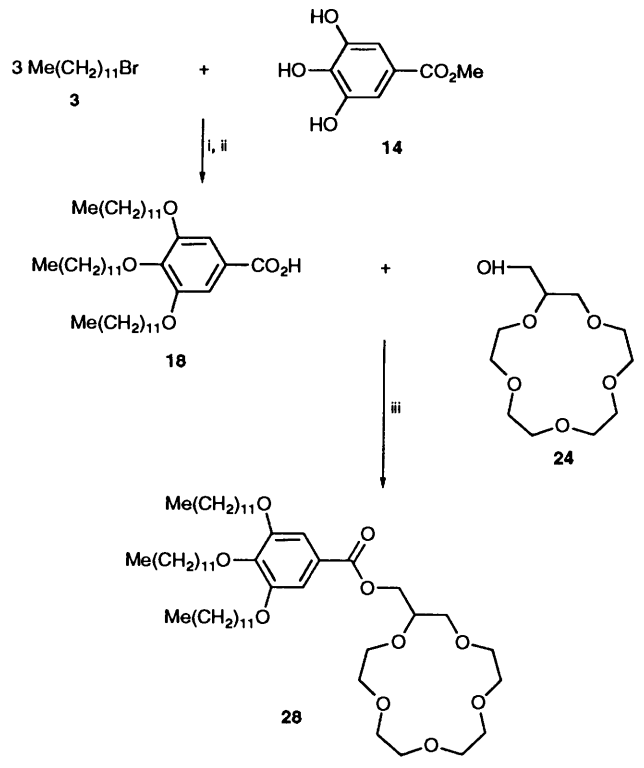

Scheme 2 Synthesis of compound **28**. *Reagents and conditions:* i, K_2CO_3, DMF, 60 °C; ii, 1 mol dm^{-3} NaOH/95% EtOH; iii, K_2CO_3, *p*-TsCl, DMAP, TBAH, THF, room temp.

phase behaviour of the complexes follows the same general trend which is determined by the size of the cation and receptor and by the amount of the salt present in the complex.

The phase transition temperatures and corresponding enthalpies of transition determined by DSC for compound **25** and its complexes with $NaCF_3SO_3$ are listed in Table 1. Compound **25** is crystalline and melts into an isotropic liquid at 68 °C. However, on the cooling and subsequent heating scan, it fails to crystallize during the kinetically controlled crystallization process which is very slow compared to the time scale of a DSC experiment. The complexes of **25** with $NaCF_3SO_3$ are also crystalline. The existence of two crystalline transitions was verified by optical microscopy. Upon heating, the complex of **25** with 0.2 mol $NaCF_3SO_3$ melts (T_{k1-k2}) at 68 °C into a biphasic mixture composed of an isotropic liquid and a second crystalline phase. Upon heating the sample above 128 °C, the second crystalline phase melts (T_{k2-i}) into a homogeneous isotropic liquid. After cooling the complexes of **25** with 0.2 and 0.4 mol $NaCF_3SO_3$ to 85 °C and annealing for 4 h, the isotropic liquid persisted. Upon cooling to room temperature, the complexes of **25** with 0.2 and 0.4 mol $NaCF_3SO_3$ crystallized (T_{k2-i}). All of the complexes had a glass transition temperature (T_g) near 0 °C.

The dependence of the transition temperatures of **25** and of the complexes of **25** with $NaCF_3SO_3$ determined by DSC during the first heating, first cooling, and second heating scans is plotted in Fig. 1. As the concentration of $NaCF_3SO_3$ is increased, T_{k2-i} increases to a maximum value at a $NaCF_3SO_3$/**25** molar ratio of 0.8 and then decreases slightly. At the same time, T_{k1-k2} shows a decrease. T_g Increases with increasing $NaCF_3SO_3$/**25** molar ratio to a constant value above a $NaCF_3SO_3$/**25** molar ratio of 1.0.

The phase transitions and corresponding enthalpy changes of transition determined by DSC of **26** and its complexes with $NaCF_3SO_3$ are shown in Table 2. Compound **26** is crystalline and melts into an isotropic liquid at 78 °C. It does not crystallize

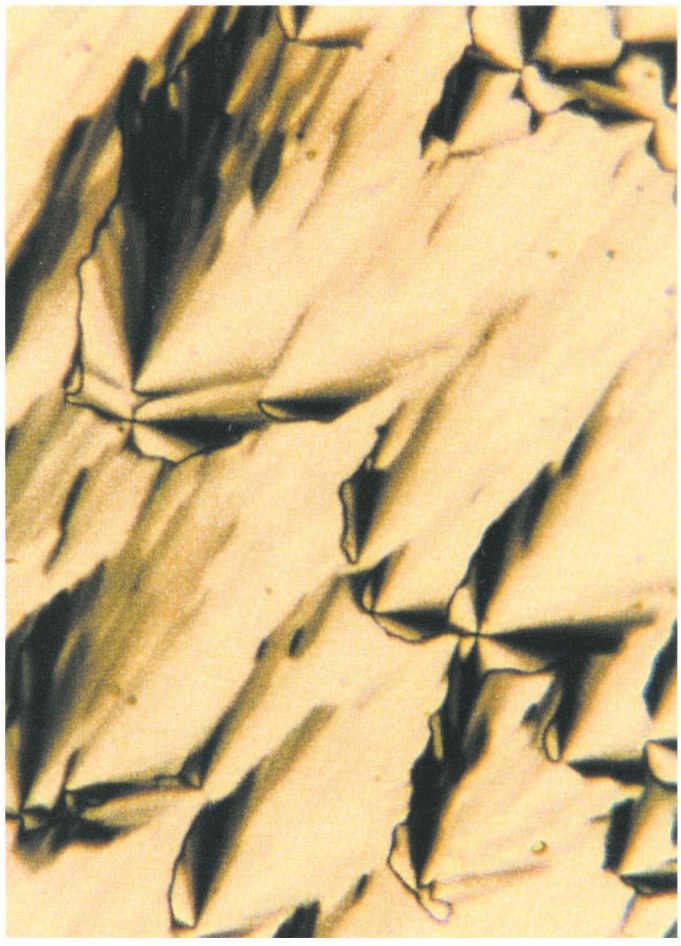

Plate I Representative optical polarized micrograph of the texture exhibited by the hexagonal columnar (Φ_h) mesophase of the complex of **27** with $NaCF_3SO_3$ (1:1 molar ratio) at 126 °C on the cooling scan

[Facing p. 453]

on cooling, but during the second heating scan, a crystallization exotherm followed by a melting endotherm is observed. The complexes of **26** with 0.2–0.6 mol $NaCF_3SO_3$ are crystalline, but only a T_g is observed above this concentration. On cooling, a T_g is observed over the entire composition range. The dependence of the phase transitions of **26** and its complexes with $NaCF_3SO_3$ on the $NaCF_3SO_3$/**26** molar ratio determined during the first heating scan, the first cooling scan, and the second heating DSC scans are plotted in Fig. 2. The crystalline melting transition (T_{k2-i}) decreases with increasing $NaCF_3SO_3$/**26** molar ratio and eventually disappears above a

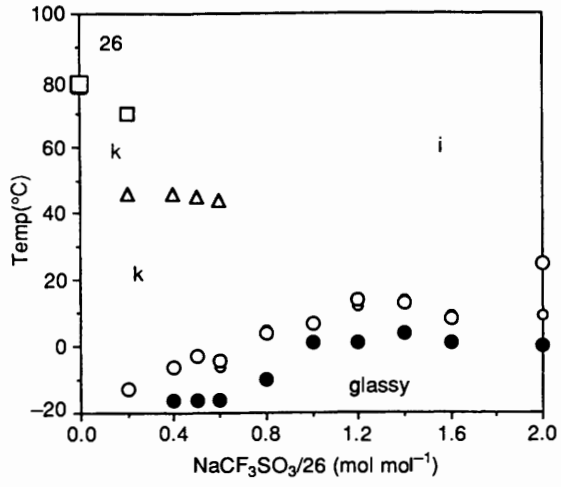

Fig. 2 The dependence of the phase transition temperatures of the complexes of **26** with $NaCF_3SO_3$ on the $NaCF_3SO_3$/**26** molar ratio. Data from the first heating scan: ○ T_g; △ T_{k1-k2}; □ T_{k2-i}. Data from the first cooling scan: ● T_g. Data from the second heating scan: ○ T_g; □ T_{k2-i}.

$NaCF_3SO_3$/**26** molar ratio of 0.6. The T_g increases with the $NaCF_3SO_3$/**26** molar ratio to a nearly constant value at a $NaCF_3SO_3$/**26** molar ratio of 1.0. The complexes of **26** with 0.4, 0.5 and 0.6 mol $NaCF_3SO_3$ were also characterized by thermal optical polarized microscopy. After cooling to a temperature below T_{k2-i} but above the T_g, no hexagonal columnar (Φ_h) mesophase was observed.

The transition temperatures and corresponding enthalpy changes of transition determined by DSC of **27** and its complexes with $NaCF_3SO_3$ are shown in Table 3. Fig. 3 presents representative DSC thermograms of **27** and its complexes with $NaCF_3SO_3$ from the first heating [Fig. 3(*a*)], the first cooling [Fig. 3(*b*)], and the second heating [Fig. 3(*c*)] scans. All subsequent heating and cooling scans were identical. Compound **27** is crystalline and melts into an isotropic liquid at 60 °C. Upon cooling, it crystallizes and then melts into an isotropic liquid during the second heating scan. The complexes of **27** with 0.2–0.4 mol of $NaCF_3SO_3$ are crystalline and exhibit a monotropic Φ_h mesophase. The complexes with 0.5–0.8 mol of $NaCF_3SO_3$ are crystalline and exhibit an enantiotropic Φ_h mesophase. Complexes of **27** with 1.0–2.0 mol of $NaCF_3SO_3$ display crystal meltings only during the first heating scan. On subsequent cooling and heating scans, they exhibit a T_g and an enantiotropic Φ_h mesophase.

The Φ_h mesophase of the complexes of **27** with $NaCF_3SO_3$ was characterized by optical polarized microscopy and X-ray scattering experiments which will be discussed in the second part. A representative texture of the Φ_h mesophase of the complex of **27** with 1.6 mol of $NaCF_3SO_3$ is shown in Plate I. The Φ_h mesophases of the complexes of **27** with $NaCF_3SO_3$ are characterized by either a fan shaped or a focal conic texture. The dependence of the crystalline-Φ_h ($T_{k-\Phi h}$) and the Φ_h-isotropic ($T_{\Phi h-i}$) transition temperature (from the first and second heating scans) and the T_g (from the second heating scan) on the

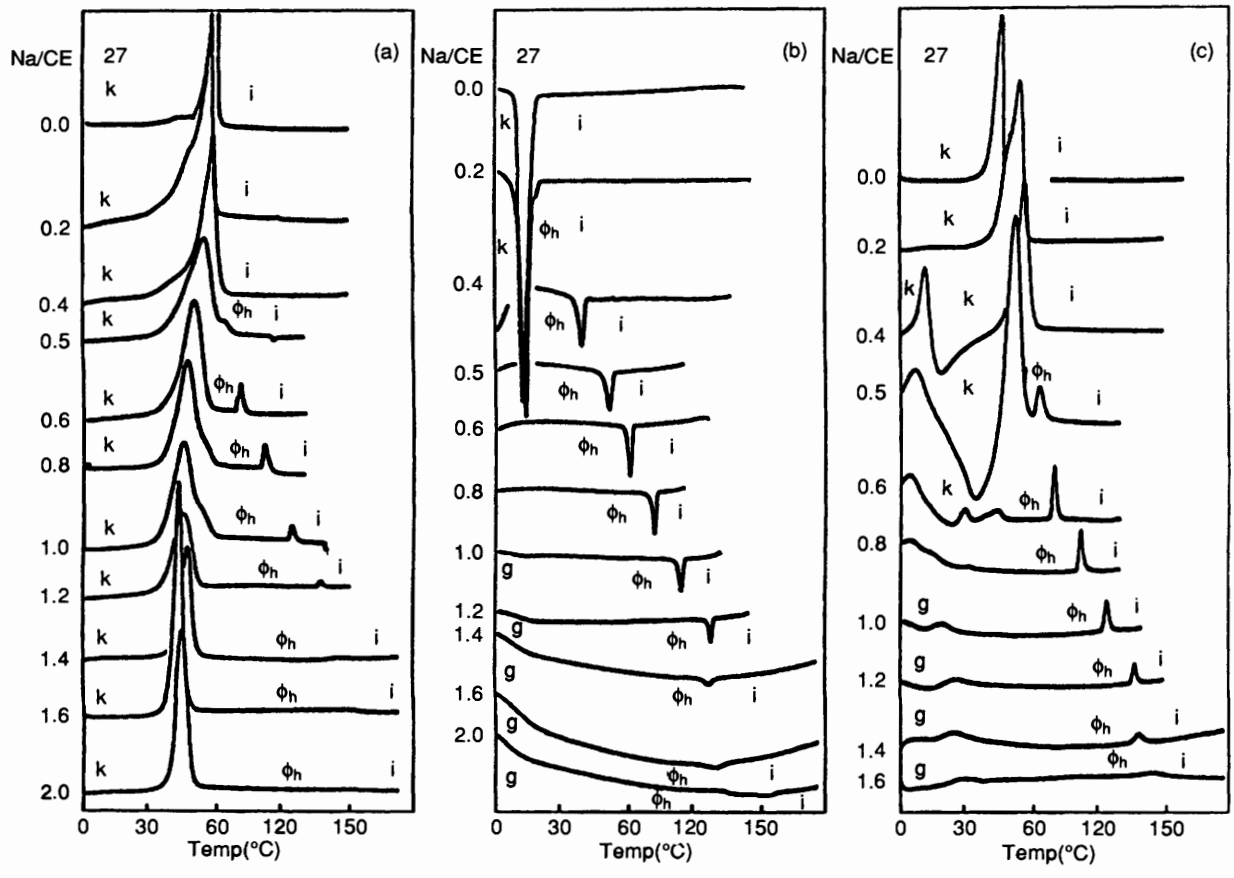

Fig. 3 DSC traces (20 °C min^{-1}) of the complexes of **27** with $NaCF_3SO_3$ recorded during: (*a*) the first heating scan; (*b*) the first cooling scan; (*c*) the second heating scan

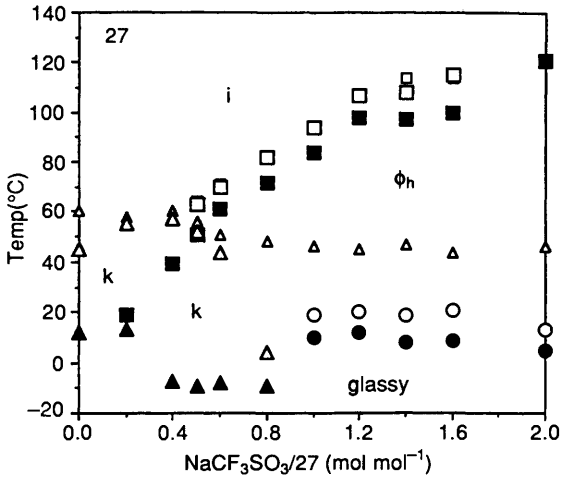

Fig. 4 The dependence of the phase transition temperatures of the complexes of **27** with $NaCF_3SO_3$ on the $NaCF_3SO_3$/**27** molar ratio. Data from the first heating scan: △ $T_{k-\Phi h}$; □ $T_{\Phi h-i}$. Data from the first cooling scan: ■ $T_{i-\Phi h}$; ▲ $T_{\Phi h-k}$, ● T_g. Data from the second heating scan: ○ T_g; △ $T_{k-\Phi h}$; □ $T_{\Phi h-i}$.

$NaCF_3SO_3$/**27** molar ratio is plotted in Fig. 4. The dependences of the T_g, isotropic-Φ_h ($T_{i-\Phi h}$), and Φ_h-crystalline ($T_{\Phi h-k}$) transition temperatures on the $NaCF_3SO_3$/**27** molar ratio from the cooling scan are plotted on the same graph. All heating and cooling scans demonstrate that the $T_{\Phi h-i}$ increases with increasing salt concentration. On cooling, $T_{\Phi h-k}$ is accompanied by a large supercooling. As the $NaCF_3SO_3$ concentration is increased, both the $T_{k-\Phi h}$ (during the second heating scan) and the $T_{\Phi h-k}$ (during the cooling scan) initially increase but then decrease with increasing $NaCF_3SO_3$ concentration. At a $NaCF_3SO_3$/**27** molar ratio of 1.0, crystallization does not occur and a T_g is observed. The T_g remains nearly constant over the entire composition range.

The transition temperatures and corresponding enthalpy changes of transition determined by DSC of **28** and its complexes with $NaCF_3SO_3$ are shown in Table 4. Compound **28** is crystalline and melts into an isotropic liquid at 32 °C. All the complexes of **28** exhibit multiple crystalline melting transitions on the first and second heating scans. Upon cooling from the isotropic melt, the complexes of **28** with 0.2–0.4 mol of $NaCF_3SO_3$ crystallize with a large supercooling. The complexes with 0.5–1.6 mol of $NaCF_3SO_3$ exhibit a $T_{i-\Phi h}$ followed by $T_{\Phi h-k}$ at lower temperatures. The complex of **28** with 2.0 mol of $NaCF_3SO_3$ does not exhibit a $T_{i-\Phi h}$ during the cooling scan. Attempts to observe a mesophase by optical polarized microscopy were inconclusive due to the presence of a crystalline phase in the isotropic melt, most probably arising from 'precipitated' free $NaCF_3SO_3$.

Fig. 5 plots the dependence of the $T_{i-\Phi h}$ and the $T_{\Phi h-k}$ of **28** and its complexes with $NaCF_3SO_3$ on the $NaCF_3SO_3$/**28** molar ratio obtained during the first cooling scan. The Φ_h mesophase of the complexes of **28** with $NaCF_3SO_3$ appears only during the cooling scan and, therefore, it is a monotropic Φ_h mesophase. Upon increasing the concentration of $NaCF_3SO_3$, $T_{i-\Phi h}$ increases while $T_{\Phi h-k}$ increases only slightly. At a $NaCF_3SO_3$/**28** molar ratio of 0.5, the $T_{i-\Phi h}$ is very close to $T_{\Phi h-k}$. Most likely, below a $NaCF_3SO_3$/**28** molar ratio of 0.5, the Φ_h mesophase is virtual.

The phase behaviour of **25**, **26**, **27** and **28** is strongly dependent on the nature of the crown ether *endo*-receptor and on the nature and length of the 'alkyl tails' of the tapered *exo*-receptor. The macroreceptors discussed in this experiment (**25**, **26**, **27**, **28**) have all been derived from a flexible (15-crown-5)-hydroxymethyl *endo*-receptor. However, they differ in the

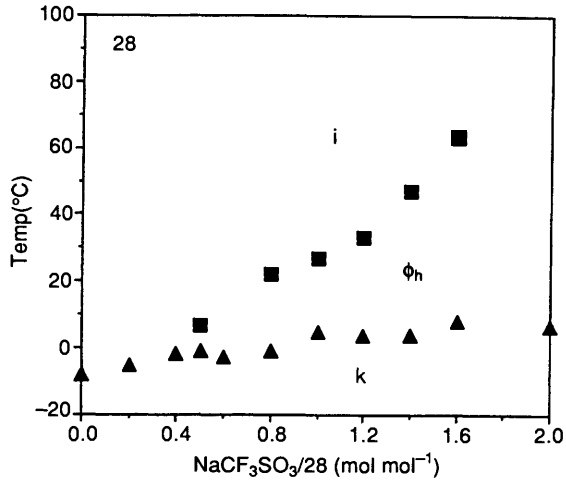

Fig. 5 The dependence of the phase transition temperatures of the complexes of **28** with $NaCF_3SO_3$ on the $NaCF_3SO_3$/**28** molar ratio. Data from the first cooling scan: ■ $T_{i-\Phi h}$; ▲ $T_{\Phi h-k}$.

nature and lengths of their alkyl tails: **25** (n = 3; Scheme 1), **26** (n = 5; Scheme 1), and **27** (n = 11; Scheme 1), derived from the 3,4,5-tris(*p*-alkoxybenzyloxy)benzoic acid tapered *exo*-receptor, differ only in the length of the alkoxy substituent. Compound **28** (n = 11; Scheme 2), derived from the 3,4,5-tris(*p*-dodecyloxy)benzoic acid tapered *exo*-receptor, lacks the benzyl ether moiety in the alkoxy substituent but is structurally similar to **27** in all other respects. A previous publication [1] described the phase behaviour of (benzo-15-crown-5)-4′-methylbenzo 3,4,5-tris(*p*-dodecyloxybenzyloxy)benzoate (**DCE**) and its complexes with $NaCF_3SO_3$. **DCE** differs from **27** only in the nature of the crown ether *endo*-receptor.

The effect of the alkyl tail length on the phase behaviour of the macroreceptor series can be most easily elucidated by analysing the phase behaviour of **25**, **26** and **27** and their complexes with $NaCF_3SO_3$. Compounds **25**, **26** and **27** are crystalline and melt (T_i) into an isotropic liquid at 67, 78 and 60 °C, respectively. The corresponding enthalpies of transition (ΔH_i) are 11.3, 15.3 and 18.3 kcal mol^{-1}, respectively. Considering $T_i = \Delta H_i/\Delta S_i$ where ΔS_i is the corresponding entropy change of transition for isotropization, the trend for the series n = 3, 5, 11 is as expected. As the lengths of the alkyl tails increase, the corresponding ΔH_i and ΔS_i are also increasing. However, the increase in ΔS_i with increasing alkyl tail length from n = 3 to n = 11 is greater than the corresponding ΔH_i due to the increased conformational combinations. Therefore, a maximum value of the T_i as a function of the alkyl tail length is observed followed by a decrease in T_i with increasing alkyl tail length.

The complexes of **25**, **26** and **27** with $NaCF_3SO_3$ are all crystalline. However, the kinetics of crystallization are such that the complexes of **25** and **26** do not crystallize during DSC analysis at a cooling rate of 20 °C min^{-1} (Tables 1 and 2). On the other hand, the complexes of **27**, which has the longest alkyl tail (n = 11), do crystallize on subsequent cooling and heating scans (Table 3, Fig. 3). Only at $NaCF_3SO_3$/**27** molar ratios greater than 0.8 is crystallization suppressed. The complexes of **25** and **26** with $NaCF_3SO_3$ do not exhibit a Φ_h mesophase while those of **27** do. This also is a consequence of the length of the alkyl tails. The shorter alkyl tails of **25** (n = 3) and **26** (n = 5) disorder at a higher temperature than the alkyl tails of **27** (n = 11) owing to the thermodynamic considerations discussed above. The formation of the Φ_h mesophase requires that the disordering temperature of the alkyl tails be lower than the temperature required for the formation of the Φ_h mesophase.[14] This requirement is met only for the longer alkyl tails of the complexes of **27**. Alkyl tail lengths from n = 6 to n = 10 have not been investigated.

Table 1 Characterization of the complexes of **25** with sodium triflate ($NaCF_3SO_3$). Data on the first lines under heating are determined during the first heating scan. Data on the second line under heating are determined during the second heating scan

Na/CE (mol mol^{-1})	Phase transitions (°C) and corresponding enthalpy changes (kcal mol^{-1})	
	Heating	Cooling
0	k 67 (11.3) i	
0.2	k_1 66 (5.25) k_2 128 (6.05) i	
0.4	k_1 64 (2.35) k_2 135 (9.59) i	i 0 g
0.5	k_1 60 (0.47) k_2 140 (11.9) i	i 1 g
	g 11 i	
0.6	k 141 (13.1) i	i 3 g
	g 10 k 137 (0.09) i	
0.8	k_1 67 (1.55) k_2 137 (12.9) i	i 9 g
	g 14 i	i 11g
1.0	k_1 81 (3.69) k_2 135 (13.1) i	
	g 19 i	i 15 g
1.2	k_1 91 (7.36) k_2 130 (13.0) i	
	g 24 i	i 15 g
1.6	k_1 110 (13.3) k_2 134 (16.2) i	
	g 24 i	i 15 g
2.0	k_1 106 (18.6) k_2 131 (11.8) i	
	g 25 i	

Table 2 Characterization of the complexes of **26** with sodium triflate ($NaCF_3SO_3$). Data on the first lines under heating are determined during the first heating scan. Data on the second line under heating are determined during the second heating scan

Na/CE (mol mol^{-1})	Phase transitions (°C) and corresponding enthalpy changes (kcal mol^{-1})	
	Heating	Cooling
0	k 78 (15.3) i	
	−k 55 (1.70) k 79 (1.73) i	
0.2	k_1 46 (8.42) k_2 70 (1.29) i	i −21 g
	g −13 i	
0.4	k 46 (8.09) i	i −16 g
	g −6 i	
0.5	k 45 (2.31) i	i −16 g
	g −3 i	
0.6	g −6 k 44 (1.05) i	i −16 g
	g −4 i	
0.8	g 5 i	i −10 g
	g 4 i	
1.0	g 7 i	i 1 g
	g 7 i	
1.2	g 12 i	i 1 g
	g 14 i	
1.4	g 14 i	i 4 g
	g 13 i	
1.6	g 9 i	i 1 g
	g 8 i	
2.0	g 9 i	i O g
	g 25 i	

The effect of incorporating a benzyl ether moiety in the alkyl tail can be studied by comparison of compounds **27** and **28** and their complexes with $NaCF_3SO_3$. Both **27** and **28** and their complexes with $NaCF_3SO_3$ are crystalline. However, the complexes of **27** with greater than 0.4 mol $NaCF_3SO_3$ display an enantiotropic Φ_h mesophase while the complexes of **28** with greater than 0.4 mol of $NaCF_3SO_3$ display only a monotropic Φ_h mesophase. Most importantly, incorporation of the benzyl ether moiety leads to an increase in the mesophase thermal stability as evidenced by the higher $T_{i-\Phi h}$ (~ 50 °C) transition temperature.

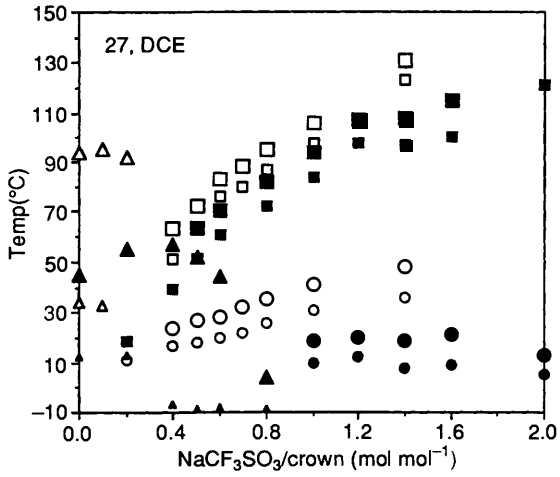

Fig. 6 Comparison of the dependence of the phase transition temperatures of the complexes of **27** with $NaCF_3SO_3$ on the $NaCF_3SO_3$/**27** molar ratio and of the complexes of **DCE** with $NaCF_3SO_3$ on the $NaCF_3SO_3$/**DCE** molar ratio. (*a*) Data from the cooling scan of **27**: ■ $T_{i-\Phi h}$; ▲ $T_{\Phi h-k}$; ● T_g. (*b*) Data from the second heating scan of **27**: ● T_g; ▲ $T_{k-\Phi h}$; ■ $T_{\Phi h-i}$. (*c*) Data from the cooling scan of **DCE**: □ $T_{i-\Phi h}$; △ $T_{\Phi h-k}$; ○ T_g. (*d*) Data from the second heating scan of **DCE**: ○ T_g; △ $T_{k-\Phi h}$; □ $T_{\Phi hi}$.

The (15-crown-5)hydroxymethyl *endo*-receptor **24** chosen for this study is similar to the previously discussed[1] benzo(15-crown-5)-4′-hydroxymethyl *endo*-receptor. However, the absence of the benzene ring in **24** should increase its conformational flexibility without greatly affecting its complexing ability. Fig. 6 plots the dependence of the $T_{k-\Phi h}$, $T_{\Phi h-i}$, and T_g of **27**, **DCE**, and their complexes with $NaCF_3SO_3$ determined from the second heating DSC scans as a function of the $NaCF_3SO_3$/crown ether molar ratio. The $T_{i-\Phi h}$, $T_{\Phi h-k}$, and T_g from the first cooling scans are plotted on the same Figure. The complexes of **DCE** exhibit a $T_{k-\Phi h}$ only during the first heating scan (not shown) and on cooling and subsequent heating they do not crystallize. Also, $T_{\Phi h-i}$, of the complexes of **DCE** is ~ 20 °C higher than that of the corresponding complexes of **27** with $NaCF_3SO_3$. The incorporation of the more flexible (15-crown-5)-hydroxymethyl *endo*-receptor (*i.e.*, **27**) results in faster crystallization kinetics while the more rigid benzo(15-crown-5)-4′-hydroxymethyl *endo*-receptor (*i.e.*, **DCE**) suppresses crystallization and increases the Φ_h mesophase thermal stability.

The complexes of **27** and **28** with 1.6 mol of $NaCF_3SO_3$ (*i.e.*, **27·1.6** and **28·1.6**) were characterized by small and wide-angle X-ray scattering. The characterization of **DCE** and its complexes with 0.6 mol of $NaCF_3SO_3$ (**DCE·0.6**) by X-ray scattering was described in detail in a previous publication.[1] Compounds **27·1.6** and **28·1.6** were characterized in the Φ_h mesophase and below the melting temperatures. The d spacings of all reflections are presented in Table 5 together with the lattice parameter (*a*), the column radius (*R*), and the hexagonal column side length (*S*). In their Φ_h mesophase, **27·1.6** and **DCE·0.6** have X-ray reflections in the ratio $d_0:d_1:d_2 = 1:1/\sqrt{3}:1/2$, with only a diffuse scattering at wide angles. This is indicative of a Φ_h mesophase.[1,15] For **28·1.6** only two sharp reflections have been observed corresponding to the spacings 42.1 and 20.6 Å in the small angle and a wide angle diffuse scattering at 4.5 Å which is indicative of a liquid crystalline mesophase. Although only two reflections were observed at low angles, with spacings in the 2:1 ratio it is most likely that this phase is Φ_h. The Φ_h phase should also exhibit a reflection with spacing $1/\sqrt{3}$ that of the first reflection. That it is not observed here is probably due to its low intensity. We note that the 20.6 Å reflect is also very weak. Furthermore, the *d* spacing of the first reflection, indexed as d_{100} is in the expected

Table 3 Characterization of the complexes of **27** with sodium triflate ($NaCF_3SO_3$). Data on the first lines under heating are determined during the first heating scan. Data on the second line under heating are determined during the second heating scan

Na/CE (mol mol^{-1})	Phase transitions (°C) and corresponding enthalpy changes (kcal mol^{-1})	
	Heating	Cooling
0	k 60 (18.3) i k 45 (16.0) i	i 12 (15.4) k
0.2	k_1 58 (18.3) i k_2 55 (14.3) i	i 19 (0.47) Φ_h 13 (11.4) k_1
0.4	k 60 (16.0) i k_1 6 (5.60) k_{-1} 18 (3.28) k_2 57 (11.6) i	i 39 (0.34) Φ_h −7 (3.03) k
0.5	k 56 (15.6) Φ_h 64 (0.68) i k_1 7 (2.29) k_{-1} 35 (1.64) k_2 52 (2.81) Φ_h 63 (0.23) i	i 51 (0.28) Φ_h −9 (0.85) k
0.6	k 51 (14.1) Φ_h 71 (9.95) i k_1 5 (2.05) k_2 30 (0.11) k_3 44 (0.11) Φ_h 70 (0.25) i	i 61 (0.23) Φ_h −8 (0.61) k
0.8	k 48 (13.4) Φ_h 82 (0.92) i k 4 (2.30) Φ_h 82 (0.23) i	i 72 (0.22) Φ_h −9 (0.31) k
1.0	k 46 (14.3) Φ_h 94 (0.39) i g 19 (0.12) Φ_h 94 (0.17) i	i 84 (0.18) Φ_h 10 g
1.2	k 45 (9.41) Φ_h 107 (0.17) i g 20 Φ_h 107 (0.09) i	i 98 (0.09) Φ_h 12 g
1.4	k 47 (9.0) Φ_h 114 (0.13) i g 19 Φ_h 108 (0.03) i	i 97 (0.07) Φ_h 8 g
1.6	k 44 (14.5) Φ_h 114* (−) i g 21 Φ_h 115 (0.06) i	i 100 (0.07) Φ_h 9 g
2.0	k 46 (11.3) Φ_h 94* (−) i g 13 Φ_h* (−) i	i 121 (0.03) Φ_h 5 g

* Observed by optical polarized microscopy.

Table 4 Characterization of the complexes of **28** with sodium triflate ($NaCF_3SO_3$). Data on the first lines under heating are determined during the first heating scan. Data on the second line under heating are determined during the second heating scan

Na/CE (mol mol^{-1})	Phase transitions (°C) and corresponding enthalpy changes (kcal mol^{-1})	
	Heating	Cooling
0	k 32 (24.5) i k_2 7 (12.8) k_{-2} 16 (5.66) k_3 32 (6.81) i	i −8 (13.3) k
0.2	k_1 7 (0.49) k_2 38 (13.2) k_3 37 (2.70) i k_1 2 (3.60) k_2 18 (8.63) i	i −5 (11.9) k
0.4	k_1 9 (1.75) k_2 37 (7.75) k_3 59 (6.39) i k_2 22 (11.7) k_{-2} 33 (3.08) k_3 54 (3.31) i	i −2 (11.5) k
0.5	k_1 9 (5.13) k_3 61 (10.2) i k_1 3 (1.33) k_2 23 (8.88) k_{-2} 32 (7.50) k_3 56 (7.72) i	i 7 (0.34) Φ_h −1 (10.0) k
0.6	k_1 10 (3.12) k_2 36 (5.36) k_3 60 (7.54) i k_2 23 (12.0) k_{-2} 33 (4.11) k_3 55 (5.02) i	i −3 (11.3) k
0.8	k_1 8 (2.39) k_3 66 (15.2) i k_2 27 (10.0) k_{-2} 38 (11.9) k_3 60 (11.2) i	i 22 (0.08) Φ_h −1 (9.17) k
1.0	k_2 33 (0.32) k_3 69 (18.7) i k_2 29 (7.79) k_2 39 (12.6) k_3 62 (13.0) i	i 27 (0.06) Φ_h 5 (7.51) k
1.2	k 69 (19.2) i k_2 31 (7.87) k_{-2} 37 (8.02) k_3 61 (8.31) i	i 33 (0.07)Φ_h 4 (5.78) k
1.4	k_2 34 (0.84) k_3 68 (18.1) i k_2 31 (6.76) k_{-2} 35 (3.99) k_3 61 (6.93) i	i 47 (0.06) Φ_h 4 (4.14) k
1.6	k_2 34 (0.85) k_{-2} 41 (0.44) k_3 68 (17.4) i k_2 31 (5.34) k_{-2} 38 (6.84) k_3 62 (6.78) i	i 63 (0.07) Φ_h 8 (5.17) k
2.0	k_2 33 (0.80) k_3 67 (17.8) i k_1 18 (0.77) k_2 29 (5.26) k_{-2} 34 (6.67) k_3 60 (8.63) i	i 7 (6.40) k

range for a Φ_h phase of similar compounds. Both **27·1.6** and **28·1.6** also display sharp crystal reflections in the Φ_h mesophase that correspond exactly with those of $NaCF_3SO_3$.

The crystalline phases of **27·1.6** and **28·1.6** were also characterized by X-ray scattering experiments. The phase is crystalline, as indicated by a number of comparatively sharp reflections extending to wide angles. These are significantly sharper than diffuse amorphous halos but, apart from the first four reflections, are broad in comparison with highly ordered crystals. Since their width does not increase significantly with diffraction angle, it would appear that small grain size is the dominant cause of broadening.

The lowest angle reflection is very strong. The first four reflections index on a hexagonal lattice, with a unit cell parameter $a = 61.7 \pm 0.03$ Å. The others are mostly *hkl* reflections. This hexagonal crystalline order is unique to **27·1.6** and has not been observed in **DCE·0.6** or in the crystalline phases of the molecular assemblies derived from oligooxyethylene glycol and 3,4,5-tris(*p*-dodecyloxybenzyloxy)benzoic acid.[2c] The fact that the hexagonal lattice parameter, *a*, is virtually identical in the two phases of **27·1.6** strongly suggests that the alkyl tails are melted in both phases. The hexagonal order is maintained within the crystalline phase of **27·1.6** owing to the increased conformational flexibility of the 15-crown-5 *endo*-receptor which resides at the centre of the supramolecular assembly. This flexibility should lead to stronger complexes

Table 5 Characterization of the complexes **DCE**,[1] **27** and **28** with sodium triflate by small-angle X-ray scattering

Compound	Na/CE (mol mol^{-1})	T (°C)	d^{hex}_{100} (Å)	d^{hex}_{110} (Å)	d^{hex}_{200} (Å)	$\langle d^{hex}_{100}\rangle$ (Å)	a (Å)	R (Å)	S (Å)	$(R + S)/2$ (Å)	ρ (g/cm^3)	μ
DCE·0.6	0.6	66	49.0	28.1	25.1	49.3	56.9	28.5	32.9	30.7	1.09	5.8
27·1.6	1.6	28	52.9	31.8	26.2	53.5	61.8	30.9	35.7	33.3		
		70	52.9	30.6	26.2	52.7	60.9	30.4	35.0	32.7	1.15	5.5
28·1.6	1.6	59	42.1	—	20.6	41.6	—	24.0*	27.7*	25.9*		

Macrocycles†	**DCE·0.6** $R_{ext.}$ (Å)	R_{core} (Å)	$E_{exp.}$ (Å)	% Shrink.	**27·1.6** $R_{ext.}$ (Å)	R_{core} (Å)	$R_{exp.}$ (Å)	% Shrink.	**28·1.6** $E_{ext.}$ (Å)	R_{core} (Å)	$R_{exp.}$ (Å)	% Shrink.
Four macrocycles	38.9	23.7	30.7	**54**	38.0	22.6	3.27	**35**	30.9	15.2	25.9	**32**
Five macrocycles	40.8	25.8	30.7	**67**	40.3	25.3	32.7	**51**	33.6	18.9	25.9	**52**
Six macrocycles	42.4	27.4	30.7	**78**	41.2	26.3	32.7	**57**	34.5	19.9	25.9	**59**

* Cell dimensions calculated from the d^{hex}_{100} reflection; Φ_h mesophase is indicated by polarized optical microscopy. † Calculated from molecular models constructed with CSC Chem 3D from Cambridge Software, Inc.: $\langle d^{hex}_{100}\rangle = d^{hex}_{100} + d^{hex}_{110} + \sqrt{3} + d^{hex}_{200} \times 2)/3$, $a = 2\langle d^{hex}_{100}\rangle/\sqrt{3}$, $R = \langle d^{hex}_{100}\rangle/\sqrt{3}$ and $S = 2R/\sqrt{3}$.

with the metal cations. The crystalline phase of **DCE·0.6** on the other hand is lamellar.[1] It is believed that in this case the reduced flexibility of the more conformationally rigid benzo-15-brown-5 *endo*-receptor prohibits this strong complexation within the column centre. The higher rigidity associated with the benzo-15-crown-5 moiety is further evidenced by the observation of a T_g in the complexes of **DCE** with $NaCF_3SO_3$ at substantially lower $NaCF_3SO_3$ molar ratios. Therefore, crystallization of the alkyl tails leading to the formation of lamellar crystalline order is more likely to occur.

Compound **28·1.6** is also derived from the flexible 15-crown-5 *endo*-receptor. However, in the crystalline phase, reflections corresponding to the following d spacings are observed: 56.0 Å (very strong), 28.0 Å (weak), 18.3 Å (weak), 14.1 Å (weak). The layer spacing, $\langle d^{layer}_{100}\rangle$ is 55.7 Å. From the fact that at low angles only a progression of harmonics of the intense 55.7 Å reflection is observed, we conclude that the crystal structure is dominated by layers of that periodicity. Molecular models of **28** [Fig. 7(*c*)] show that the longest dimension of the most extended molecular conformation is 31.6 Å. This suggests that the molecules form double layers with the crown ethers arranged head-to-head within the layers. Furthermore, the presence of a strong 4.1 Å and a somewhat weaker 3.9 Å reflection suggests that the aliphatic layers are ordered in a similar fashion to the layers in the crystalline[16] or the rotator[17] phase of normal paraffins.

The change from a layered to a cylindrical architecture upon crystalline melting is due to the increase in the chain cross-section upon melting of the aliphatic tails. With the aliphatic chains crystallized and extended, their joint cross-section of *ca.* $3 \times 20 = 60$ Å^2 appears to be matched by the complexed crown ether end of the molecule. However, the laterally expanded melted alkyl chains could not be sustained by flat layers, giving rise to the cylindrical arrangement of the columnar phase instead. In the latter arrangement, melted alkyl chains are believed to form the outer sheath surrounding the crown ether interior. Such a layer-column transformation has several precedents, involving either a smectic-columnar[18] or a crystal-columnar[19] transition.

In order to investigate possible molecular arrangement within the columns, molecular models were built of what is believed to be the near minimum energy conformation of isolated molecules of **27** and **28**. The values for bond lengths, bond angles, and torsion angles for the tapered *exo*-receptor portion of the models were taken from crystallographic data of related compounds and described previously.[1] The conformation of the complexed hydroxymethyl(15-crown-5) *endo*-

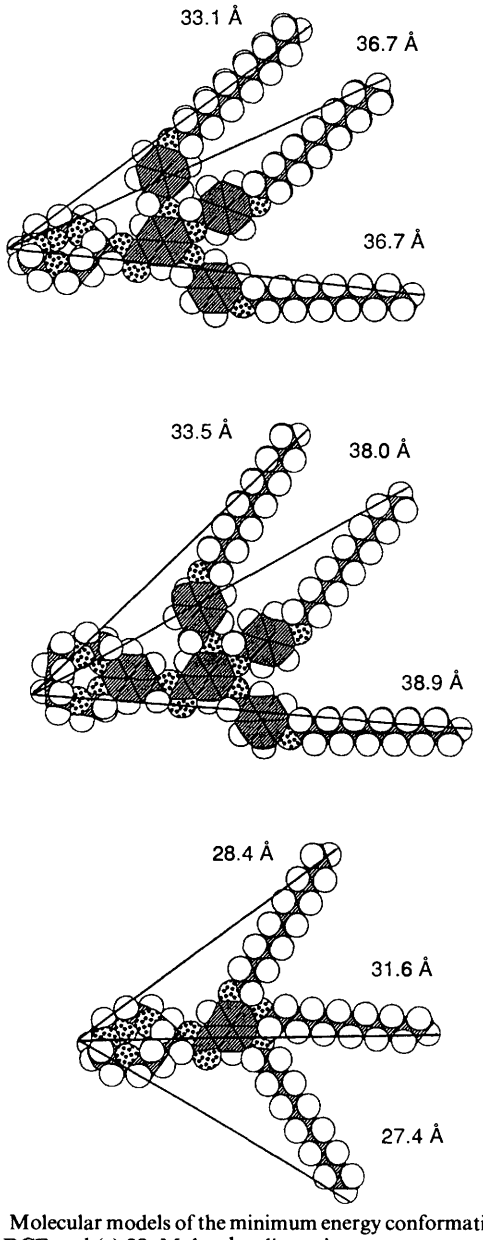

Fig. 7 Molecular models of the minimum energy conformations of: (*a*) **27**, (*b*) **DCE** and (*c*) **28**. Molecular dimensions are measured from the end surface of the outermost hydrogen on the crown ether ring to the ends of the extended aliphatic tails.

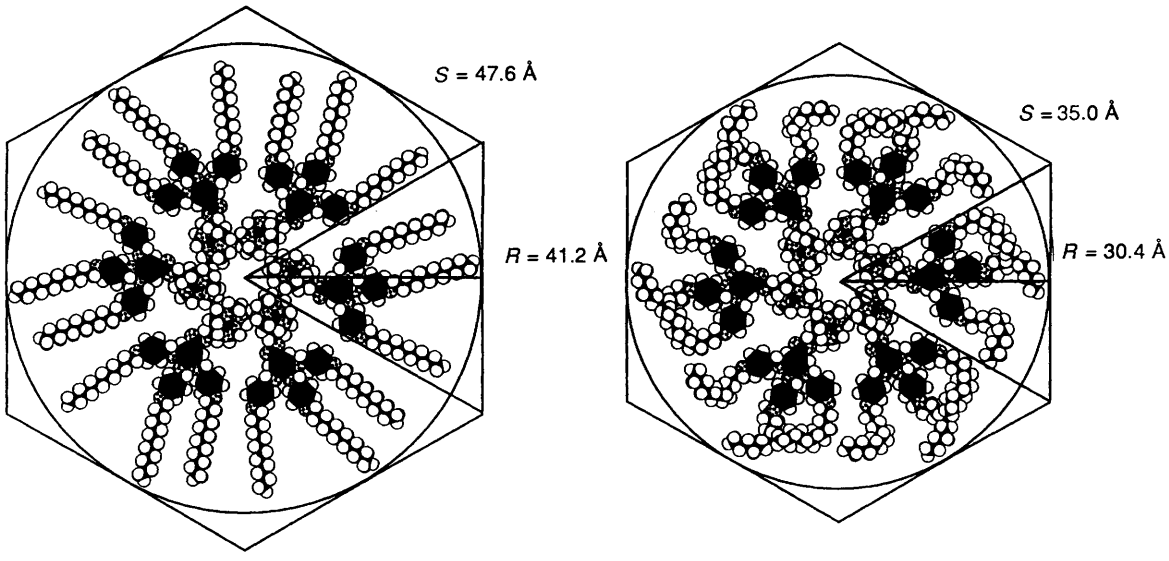

Fig. 8 Schematic representation of the column layer of **27·1.6** in the Φ_h mesophase: (*a*) top view of a layer containing six molecules of **27·1.6** with the alkyl tails extended; (*b*) top view of a layer containing six molecules of **27·1.6** with the alkyl tails melted

receptor portion was obtained from the crystallographic data of a related compound.[20] The planar conformations of **27**, **DCE** and **28** are shown in Figs. 7(*a*), (*b*) and (*c*), respectively. The key dimensions of interest are only marginally different in the planar conformation from those in the minimum energy state.

In the Φ_h mesophase of compounds with tapered molecules of similar shape as the current ones, the three aliphatic tails radiate toward the periphery of the column, while the acute apex of the tapered molecule resides near the centre.[1,2] A similar arrangement is also expected in the complexes of **27** and **28**. A representative molecular model of the top projection of an assembly of **27** consisting of six tapered units is presented in Fig. 8(*a*). Models composed of four and five structural units were also constructed and the relevant dimensions measured, but their figures have been omitted for brevity. The crown ether *endo*-receptors are centred side by side inside the column and the extended aliphatic tails radiate outward to the column periphery. The radius ($R_{ext.}$) of the column derived from the minimum energy conformation is measured from the column centre to the end of the outermost alkyl tail. The internal core radius (R_{core}) was measured from the column centre to the outermost aromatic ether oxygen atom. The model dimensions and the corresponding experimentally determined average column radii ($R_{exp.} = R + S/2$) of **27·1.6**, **DCE·0.6** and **28·1.6** from X-ray are presented in Table 5.

Comparison of $R_{ext.}$ and $R_{exp.}$ values (Table 5) provides insight into the self-assembled supramolecular architecture of **27·1.6**. The experimentally determined radius ($R_{exp.}$) falls significantly short of the extended radius measurement ($R_{ext.}$) due to the conformational melting of the alkyl tails.[1,2] If it is assumed that the difference between $R_{exp.}$ and $R_{ext.}$ is due only to the flexibility of the alkyl tails, the extent of the alkyl tail shrinkage can be determined as follows:

$$\% \text{ shrinkage} = \frac{R_{ext.} - R_{exp.}}{R_{ext.} - R_{core}} \times 100$$

$R_{ext.}$ = average measured radius from extended conformation model [Fig. 8(*a*)]; $R_{exp.}$ = average radius determined experimentally (Table 5) and R_{core} = radius of rigid aromatic core [Fig. 8(*a*)].

The alkyl tail shrinkages for the models of **27·1.6**, **28·1.6** and **DCE·0.6** are tabulated in Table 5. Arrangement of four, five and six macrocycles [Fig. 8(*a*)] within the column layer of **27·1.6** gives alkyl tail shrinkages of 35, 51 and 57%, respectively. Previous work in our laboratory[1,15b] has shown a shrinkage of as much as 55%. In the case where four macrocycles are arranged in the column layer, the alkyl tail shrinkage of 35% indicates that if the alkyl tails exist in a non-extended conformation, their length would not be sufficient to reach the column periphery. Therefore, five or six macrocycles should be required.

The alkyl tail shrinkage from the models of **DCE·0.6** are 54, 67 and 78% for four, five and six macrocycles, respectively. These values are significantly larger than the corresponding shrinkages of **27·1.6**. The experimentally determined column radius of **27·1.6** is 32.7 Å, while that of **DCE·0.6** is 30.7 Å. However, $R_{ext.}$ of the models of **DCE·0.6** are from 0.5 to 1.2 Å larger than the corresponding radii of **27·1.6**. At first glance, it would seem contradictory that the smaller macrocycle, **27**, would lead to assemblies with a larger column radius. Most probably, **27·1.6** contains on average six macrocycles per column layer which leads to a quite reasonable alkyl tail shrinkage of 57%. The arrangement of six molecules of **DCE** per column layer leads to an excessively large alkyl tail shrinkage (78%), and therefore, a model based on four (54%) or five (67%) macrocycles seems more likely. The column radius of **27·1.6** determined from X-ray scattering experiments is expected to be larger due to the presence of more macrocycles per layer.

The number of molecules (μ) of **27** or **DCE** that are present in a hexagonal prism layer of height t, can be determined from the experimentally measured density (r) of the complexes and from the experimental value of the distance from the column centre to the hexagon vertex, S:[1,21]

$$\rho = \frac{2\mu M}{\sqrt{3} N_A S^2 t}$$

The values of μ are shown in Table 5. According to this calculation, **27·1.6** and **DCE·0.6** contain 5.5 and 5.8 macrocycles per column layer, respectively.

Fig. 8(*b*) presents the most likely arrangement of a column layer in the Φ_h mesophase of **27·1.6** with the alkyl tails melted to correspond to the experimentally determined column radius. Ionic interactions between complexed and uncomplexed crown ether structural units facilitate the aggregation of six tapered molecules into a cylindrical assembly with the hydrophobic

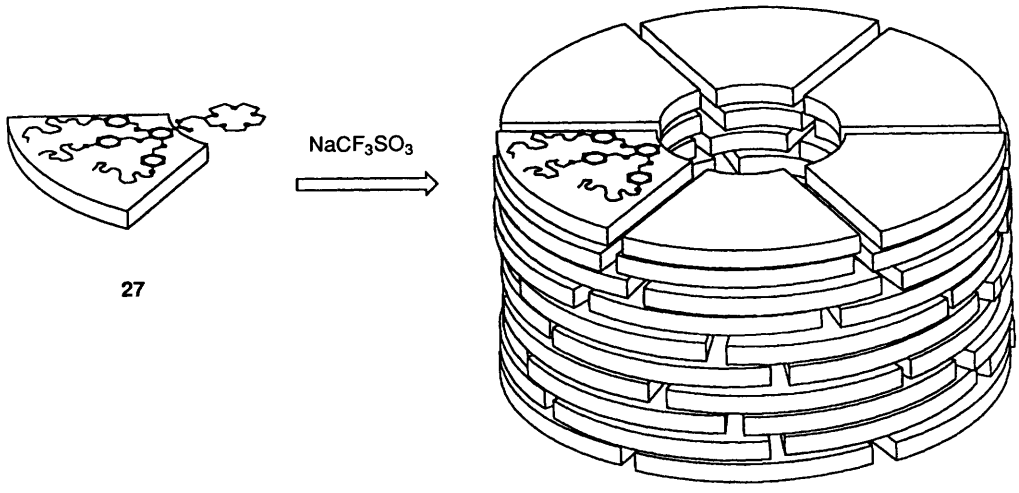

Fig. 9 Schematic representation of the self-assembly of the tapered *endo*-receptor, **27**, into a tubular molecular architecture upon complexation with $NaCF_3SO_3$

alkyl tails concentrated at the periphery. Above $T_{k-\Phi h}$ or T_g, the molecules assemble into cylinders which pack in a hexagonal arrangement producing the observed Φ_h mesophase. A similar model has been proposed[1] for **DCE·0.6** composed of five macrocycles per layer.

It is possible to construct similar molecular models of the assemblies of **28·1.6**. The experimentally determined column radius is 26.0 Å. The alkyl tail shrinkage (Table 5) is 32, 52 and 59% for assemblies consisting of four, five and six macrocycles, respectively. The fact that the shrinkage is nearly identical with the corresponding values for **27·1.6** substantiates the assumption that conformational melting is restricted to the alkyl tails. The benzyl ether moieties are more conformationally restricted and serve to stabilize the mesophase.

Fig. 9 presents a schematic representation of the self-assembly of **27** into a tubular molecular architecture upon complexation with $NaCF_3SO_3$. The flexible 15-crown-5 *endo*-receptor forms a complex with $NaCF_3SO_3$. This complexation, in turn, induces ionic interactions between complexed and uncomplexed crown ether moieties. The tapered shape of the 3,4,5-tris(*p*-dodecyloxybenzyloxy)benzoate *exo*-receptor facilitates the formation of a cylindrical assembly with the complexed crown ethers in the centre, surrounded by the melted alkyl tails in the Φ_h mesophase. This self-assembly resembles that of the tobacco mosaic virus (TMV) which has been discussed in our previous publication[1] and the references cited therein.

Acknowledgements

Financial support by the National Science Foundation (DMR-92-06781), and a NATO travelling grant are gratefully acknowledged.

References

1 V. Percec, G. Johansson, J. Heck, G. Ungar and S. V. Batty, *J. Chem. Soc., Perkin Trans. 1*, 1993, 1411.
2 (*a*) V. Percec, M. Lee, J. Heck, H. Blackwell, G. Ungar and A. Alvarez-Castillo, *J. Mater. Chem.*, 1992, **2**, 931; (*b*) V. Percec, J. Heck, M. Lee, G. Ungar and A. Alvarez-Castillo, *J. Mater. Chem.*, 1992, **2**, 1033; (*c*) V. Percec, J. Heck, D. Tomazos, F. Falkenberg, H. Blackwell and G. Ungar, *J. Chem. Soc., Perkin Trans. 1*, 1993, 2799; (*d*) V. Percec, J. Heck, D. Tomazos and G. Ungar, *J. Chem. Soc., Perkin Trans. 2*, 1993, 2381; (*e*) D. Tomazos, R. Out, J. Heck, G. Johansson, V. Percec and M. Moeller, *Liq. Cryst.*, in press.
3 T. Gramstad and R. N. Haseldine, *J. Chem. Soc.*, 1956, 173.
4 R. M. Metzer, D. C. Wiser, R. K. Laidlaw, M. A. Takassi, D. L. Mattern and C. A. Panetta, *Langmuir*, 1990, **6**, 350.
5 C. Rohmann and D. Meisel, *Arch. Pharm.*, 1961, **294**, 538.
6 H. Buckbühler, H. Büchi, J. Schreiber and A. Eschenmoser, *Helv. Chim. Acta*, 1965, **48**, 1746.
7 (*a*) J. Malthête, N. Tinh and A. M. Levelut, *J. Chem. Soc., Chem. Commun.*, 1986, 1548; (*b*) V. Percec and J. Heck, *J. Polym. Sci., Part A: Polym. Chem.*, 1991, **29**, 591.
8 P. Huszthy, M. Oue, J. S. Bradshaw, C. Y. Zhu, T. Wang, N. K. Dalley, J. C. Curtis and R. M. Izatt, *J. Org. Chem.*, 1992, **57**, 5383.
9 E. Baer and M. Kates, *J. Am. Chem. Soc.*, 1950, **72**, 942.
10 D. M. Dishong, C. J. Diamond, M. I. Cinoman and G. W. Gokel, *J. Am. Chem. Soc.*, 1983, **105**, 586.
11 M. Bourgoin, K. H. Wong, J. Y. Hui and J. Smid, *J. Am. Chem. Soc.*, 1975, **97**, 3462.
12 K. Kikukawa, G. K. He, A. Abe, T. Goto, R. Arata, T. Ikeda, F. Wada and T. Matsuda, *J. Chem. Soc., Perkin Trans. 2*, 1987, 135.
13 C. J. Pedersen, *J. Am. Chem. Soc.*, 1967, **89**, 7017.
14 (*a*) D. M. Collard and C. P. Lillya, *J. Am. Chem. Soc.*, 1991, **113**, 8578; (*b*) E. Fontes, P. G. Heiney, M. Okaba, J. N. Haseltine and A. B. Smith III, *Phys. Rev., A*, 1988, **37**, 1329.
15 (*a*) P. S. Pershan, *Structures of Liquid Crystalline Phases*, World Scientific, Singapore, 1988; (*b*) V. Percec, J. Heck and G. Ungar, *Macromolecules*, 1991, **24**, 4957.
16 A. E. Smith, *J. Chem. Phys.*, 1953, **21**, 2229.
17 G. Ungar, *J. Phys. Chem.*, 1983, **87**, 689.
18 C. Destrade, N. H. Tinh, A. Roubineau and A. M. Levelut, *Mol. Cryst. Liq. Cryst.*, 1988, **159**, 163.
19 J. Watanabe, H. Ono, I. Uematsu and A. Abe, *Macromolecules*, 1985, **18**, 2141.
20 P. Groth, *Acta Chem. Scand. A*, 1981, **35**, 721.
21 C. R. Safinya, K. S. Liang, W. A. Varady, N. A. Clark and G. Anderson, *Phys. Rev. Lett.*, 1984, **53**, 1172.

Paper 3/04558G
Received 30*th July* 1993
Accepted 23*rd September* 1993